

Weighted objective function selector algorithm for parameter estimation of SVAT models with remote sensing data

Joseph A. P. Pollacco,¹ Binayak P. Mohanty,¹ and Andreas Efstratiadis²

Received 16 December 2012; revised 11 September 2013; accepted 26 September 2013.

[1] The objective function of the inverse problem in Soil-Vegetation-Atmosphere-Transfer (SVAT) models can be expressed as the aggregation of two criteria, accounting for the uncertainties of surface soil moisture (θ) and evapotranspiration (ET), retrieved from remote sensing (RS). In this context, we formulate a Weighted-Objective-Function (WOF) with respect to model effective soil hydraulic parameters, comprising of two components for θ and ET , respectively, and a dimensionless coefficient w . Given that the sensitivity of θ is increased by omitting the periods when soil moisture decoupling occurs, we also introduce within the WOF a threshold, θ_d , which outlines the decoupling of the surface and root-zone moisture. The optimal values of w and θ_d are determined by using a novel framework, weighted objective function selector algorithm (WOFSA). This performs numerical experiments, assuming known reference conditions. In particular, it solves the inverse problem for different sets of θ and ET , considering the uncertainties of retrieving them from RS, and then runs the hydrological model to obtain the simulated water fluxes and their residuals, ΔWF , against the reference responses. It estimates the two unknown variables, w and θ_d , by maximizing the linear correlation between the WOF and maximum ΔWF . The framework is tested using a modified Soil-Water-Atmosphere-Plant (SWAP) model, under 22 contrasting hydroclimatic scenarios. It is shown that for each texture class, w can be expressed as function of the average θ and ET -fraction, while that for all scenarios θ_d can be modeled as function of the average θ , average ET , and standard deviation of ET . Based on the outcomes of this study, we also provide recommendations on the most suitable time period for soil moisture measurements for capturing its dynamics and thresholds. Finally, we propose the implementation of WOFSA within multiobjective calibration, as a generalized tool for recognizing robust solutions from the Pareto front.

Citation: Pollacco, J. A. P., B. P. Mohanty, and A. Efstratiadis (2013), Weighted Objective Function Selector Algorithm for parameter estimation of SVAT models with remote sensing data, *Water Resour. Res.*, 49, doi:10.1002/wrcr.20554.

1. Introduction

[2] In the hydrological community, there is a growing interest to make suitable usage of data retrieved from remote sensing (RS), to be employed within physically based models. Two of the most typical variables, which are of key importance in hydrological modeling, are surface soil moisture, θ [Sun *et al.*, 2007; Wang *et al.*, 2008; Zhan *et al.*, 2008; Naeimi *et al.*, 2009; Entekhabi *et al.*, 2010] and actual evapotranspiration, ET [e.g., Wang *et al.*, 2008; Wu *et al.*, 2008; Hong *et al.*, 2009; Ramos *et al.*, 2009; Teixeira *et al.*, 2009a]. In particular, RS data of this type

have been used to invert the soil hydraulic parameters of Soil-Water-Atmosphere-Plant (SVAT) models [e.g., Mohanty and Zhu, 2007; Ines and Mohanty, 2008a, 2009; Gutmann and Small, 2010]. Recently, Pollacco and Mohanty [2012] performed numerical experiments under 18 contrasting hydroclimatic scenarios to estimate the uncertainties of computing the water fluxes (WF) through a modified SVAT model, by inverting its soil hydraulic parameters from θ and ET . They found that the predictive capacity of the model against its simulated fluxes strongly depends on the hydroclimatic conditions; specifically, the uncertainty increases under dry climates, coarse textures, and deep rooted vegetation.

[3] In this paper, we provide a novel methodological framework, termed Weighted Objective Function Selector Algorithm (WOFSA), to improve predictions by SVAT models, by ensuring the most appropriate combination of these two types of information (θ and ET), for a wide range of hydroclimatic conditions and soil texture patterns. In the simulations, we use a modified SWAP 3.2 model, for which we are interested in inverting the effective soil hydraulic parameters, while the vegetation parameters are assumed known. The modified SWAP 3.2, introduced by Pollacco

¹Department of Biological and Agricultural Engineering, Texas A&M University, College Station, Texas, USA.

²Department of Water Resources and Environmental Engineering, School of Civil Engineering, National Technical University of Athens, Zographou, Greece.

Corresponding author: B. P. Mohanty, Department of Biological and Agricultural Engineering, Texas A&M University, College Station, TX 77843-2117, USA. (bmohanty@tamu.edu)

and Mohanty [2012] and next termed $SWAP_{inv}$, is briefly described in section 2.1.

[4] In the proposed framework, the inverse problem is expressed in multiobjective terms, by formulating a Weighted Objective Function (WOF) of two criteria, OF_θ and OF_{et} , which account for the deviation of the simulated to the “reference” surface soil moisture θ and evapotranspiration ET , i.e.,

$$WOF = wOF_\theta + (1 - w)OF_{et} \quad (1)$$

where w is a dimensionless weighting coefficient. Multiobjective approaches have been widely documented in all aspects of hydrological modeling, starting from the late 1990s [e.g., Mroczkowski et al., 1997; Gupta et al., 1998; Yapo et al., 1998; Bastidas et al., 1999; Gupta et al., 1999]. The rationale is that as more information is embedded within calibration, it is expected that the identifiability of parameters is improved, thus also ensuring an improved predictive capacity. These advantages have been demonstrated in several applications involving SVAT and land surface models [e.g., Bastidas et al., 1999; Franks et al., 1999; Gupta et al., 1999; Demarty et al., 2004, 2005; Coudert et al., 2006; Mo et al., 2006]. In this respect, conditioning the hydraulic parameters of SVAT models against both θ and ET data is generally accepted, although not all researchers found advantageous of calibrating SVAT models simultaneously with θ and ET data [Ines and Droogers, 2002; Jhorar et al., 2002, 2004; Ines and Mohanty, 2008b].

[5] In order to increase the information embedded in calibration, the WOF is further parameterized by introducing a threshold soil moisture θ_d , which indicates the period when soil moisture θ can be calibrated, in order to avoid decoupling between surface and subsurface θ . The concept of θ_d is one of the novelties of our framework, as explained in section 2.4.2. It is well known that by tuning the weighting coefficient w and next solving the inverse (calibration) problem for a given value of θ_d , we can obtain different sets of optimized hydraulic parameters. The later are called nondominated or Pareto-optimal and lie in the boundary of the feasible objective space (Figure 1). By assigning a specific value to w and θ_d , we assert that the solution obtained by minimizing WOF ensures an acceptable compromise between OF_θ and OF_{et} . In this respect, the “optimal” combination of θ and ET data is mathematically represented as the determination of the weighting coefficient w and the decoupled soil moisture θ_d . The Weighted Objective Function Selector Algorithm (WOFSA) is a novel numerical procedure, which allows for identifying the optimal values of both the control variables of the multiobjective function (i.e., w and θ_d) and the model hydraulic parameters. The suitability of w and θ_d is evaluated on the basis of the information provided by the simulated water fluxes (model outputs), in terms of uncertainty, in an attempt to constrain the feasible parameter space. In contrast to the classic calibration paradigm, which merely aims to achieve the smallest departure between the observed and simulated model responses, the WOFSA also takes into account the uncertainties due to errors in input data. For convenience, in the

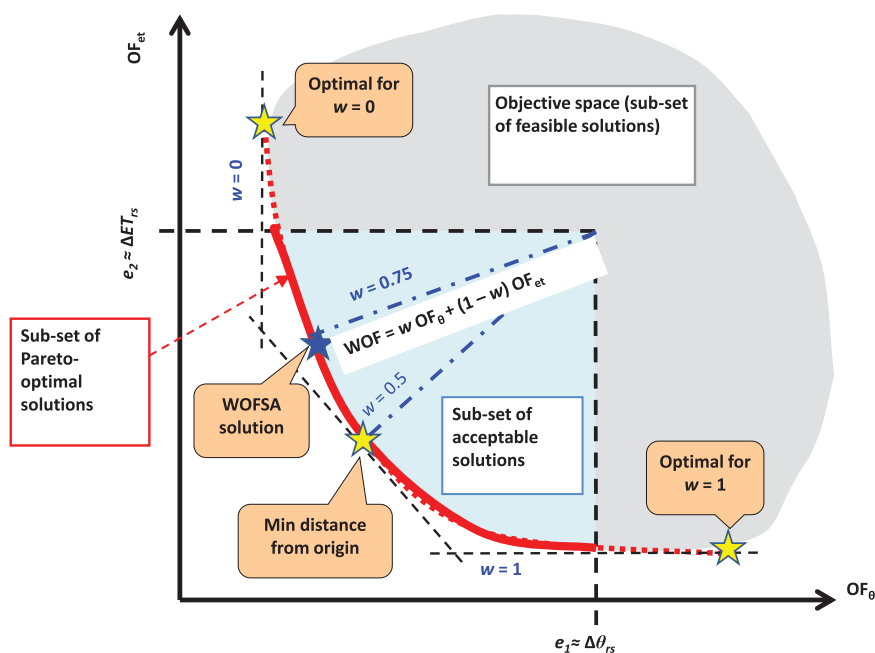


Figure 1. Graphical example illustrating the objective space, the Pareto front and characteristic solutions of a hypothetical problem of simultaneous minimization of two criteria (in the specific case OF_θ and OF_{et}). Vector $e = [e_1, e_2]$ indicates limits of acceptability (in the specific case uncertainty bounds), for distinguishing feasible solutions. Shown are the extreme solutions of the Pareto front (corresponding to $w=0$ and $w=1$), the solution that has the minimum distance from the origin and the solution provided by WOFSA, corresponding to $w=0.75$.

investigations, we use synthetic data provided by numerical experiments with known parameter sets, in order to eliminate the impacts of other sources of uncertainty, e.g., structural (model) errors. In this context, WOFSA assumes that the uncertainties of the water fluxes are only caused by prescribed uncertainties of the observed θ and ET .

[6] Specifically, we consider that the top 5 cm soil moisture retrieved from remote sensing has an average accuracy of root mean square error (RMSE) of $0.04 \text{ m}^3 \text{ m}^{-3}$, in terms of volumetric soil moisture [e.g., *Kerr et al.*, 2001; *Simmonds et al.*, 2004; *Davenport et al.*, 2005; *Choi et al.*, 2008; *Das et al.*, 2008; *Sahoo et al.*, 2008; *Verstraeten et al.*, 2008; *Vischel et al.*, 2008]. This has been validated with field campaigns, typically under low vegetated area for which the biomass is up to $4\text{--}8 \text{ kg m}^{-2}$ (for example, under mature corn and soybean), by using passive microwave remote sensing [e.g., *Jackson and Schmugge*, 1991; *Bindlish et al.*, 2006; *Li et al.*, 2006; *Njoku and Chan*, 2006]. On the other hand, the procedures for retrieving the actual evapotranspiration from remote sensing exhibit an average relative error of 20%, as also validated from field campaigns. This value is suggested by *Kalma et al.* [2008], from a compilation of 30 publications [e.g., *Zhang et al.*, 2006; *Gao and Long*, 2008; *Opoku-Duah et al.*, 2008; *Bashir et al.*, 2009; *Ramos et al.*, 2009; *Teixeira et al.*, 2009b]. We note that the uncertainties of retrieving θ are different when compared to the uncertainties of ET , and therefore have different implications on the uncertainties of the modeled/inverted water fluxes. Moreover, the behavior of the uncertainties of θ and ET retrieved from RS with increasing θ and ET is still poorly understood [e.g., *Fernández-Gálvez*, 2008]. For this reason, we also assume that the uncertainties of θ and ET linearly increase with increasing θ and ET , thus suggesting that the WOF and the corresponding residuals are correlated. Under this premise, the optimal w and θ_d are those which achieve the maximum linear correlation between the WOF and the residuals of the simulated water fluxes. This is a key point of the methodology, which is analytically presented in section 3.

[7] Our methodology is validated by employing numerical experiments with SWAP_{inv}. Following the recent research study by *Pollacco and Mohanty* [2012], we used as reference states/fluxes the surface and root-zone soil moisture, groundwater recharge, actual evapotranspiration, actual evaporation, and actual transpiration. In order to investigate the variability of the optimized w and θ_d , we formulated 22 contrasting hydroclimatic scenarios, which are composed as combination of five climates across the USA, three soil textures, and two rooting depths. The need for investigating different rooting depths is justified by *Ines and Mohanty* [2008b], who found that the predictions of the hydraulic parameters of SVAT models are much more sensitive to rooting depths than other vegetation parameters. In the numerical experiments, we assumed that the soil hydraulic parameters are unknown and that the vegetation parameters are not subject to calibration, since these can be readily retrieved from MODIS (MODerate resolution Imaging Spectroradiometer) [e.g., *Huete et al.*, 2002; *Simic et al.*, 2004; *Nagler et al.*, 2005; *Vegas Galdos et al.*, 2012]. In all simulations, we assumed that the soils are homogeneous, based on the work by *Jhorar et al.* [2004], who found that, in most cases, a reliable water balance can

be obtained by replacing the heterogeneous soil profile by an equivalent single one. Finally, we selected a deep water table, since *Pollacco and Mohanty* [2012] showed that inverting the soil hydraulic parameters with ET in the presence of shallow water table causes extra uncertainties.

[8] The goals of this study include:

[9] 1. Development of the weighted objective function selector algorithm (WOFSA) for determining the best-compromise weights of a WOF.

[10] 2. Application of WOFSA within SWAP_{inv} in order to investigate the variability of the optimal coefficient w and threshold θ_d under contrasting hydroclimatic conditions, on the basis of synthetic data obtained through numerical experiments, i.e., by inverting the soil hydraulic parameters.

[11] 3. Determination of the most suitable calibration period (in terms of soil moisture thresholds) to take full advantage of the information provided simultaneously by θ and ET retrieved from remote sensing.

[12] 4. Development of empirical relationships correlating w and θ_d against typical statistical metrics of θ and ET .

[13] 5. Comparison with the minimum Euclidian distance approach, which is usually employed in multiobjective calibration problems.

[14] 6. Discussion of future research perspectives, for implementing WOFSA within a multiobjective calibration framework, and on the basis of actual (i.e., field) data.

2. Modeling Framework and Set-Up of Numerical Experiments

2.1. Soil-Water-Atmosphere-Plant Hydrological Model

[15] We introduce a modified version of the so-called Soil-Water-Atmosphere-Plant (SWAP 3.2), which is a physically based Soil-Vegetation-Atmosphere-Transfer (SVAT) water flow model for representing the unsaturated zone soil water fluxes of vegetated land [e.g., *Van Dam et al.*, 1997; *Kroes et al.*, 2000; *Van Dam et al.*, 2008]. SWAP has been extensively used to calibrate the hydraulic parameters by matching θ and/or ET retrieved from remote sensing [e.g., *Ines and Mohanty*, 2008a, 2008b, 2008c, 2009; *Shin et al.*, 2012]. The governing equation solves the mixed form of the Richards' equation, combined with a sink term for root water extraction, to simulate the variably saturated soil moisture movement in the soil profile

$$\frac{\partial \theta}{\partial t} = \frac{\partial (K(\theta) \left(\frac{\partial h}{\partial z} + 1 \right))}{\partial z} - S(h) \quad (2)$$

where θ is the volumetric water content ($\text{L}^3 \text{ L}^{-3}$) or the fraction of water-filled pore space, h is the capillary pressure head (m), t is the time (T), z is the vertical coordinate (L) defined as positive upward, $K(\theta)$ is the unsaturated hydraulic conductivity (L T^{-1}), and $S(h)$ is the soil water extraction rate by plant roots ($\text{L}^3 \text{ L}^{-3}$).

2.1.1. Soil Water Retention and Unsaturated Hydraulic Conductivity

[16] The model accuracy depends on two functions, the soil-moisture characteristic curve $h(\theta)$ and the unsaturated

hydraulic conductivity $K(\theta)$. The analytical function of $h(\theta)$ is provided by the *van Genuchten* model [1980]

$$\theta_e = \frac{\theta - \theta_r}{\theta_s - \theta_r} \frac{1}{\left[1 + \left(\frac{h}{h_{ae}}\right)^n\right]^m} \quad (3)$$

where θ_e is the normalized volumetric water content ($L^3 L^{-3}$), θ_r and θ_s are the residual and saturated water contents ($L^3 L^{-3}$), respectively, with $0 \leq \theta_r < \theta < \theta_s$, h is the capillary pressure head (m), $h_{ae}(1/\alpha)$ is associated to the air-entry matrix potential (m^{-1}), n (>1) is a shape parameter related to the pore-size distribution (dimensionless), and m is another shape parameter. The two parameters m and n are interrelated via the expression $m = 1 - 1/n$, following the assumption by *Mualem* [1976].

[17] The unsaturated hydraulic conductivity function $K(\theta)$ is given by *Mualem* [1976] and *van Genuchten* [1980]

$$K(\theta) = K_s \theta_e^L \left[1 - \left(1 - \theta_e^m\right)^2\right] \quad (4)$$

where L is a dimensionless shape factor and K_s is the saturated hydraulic conductivity ($m d^{-1}$). The shape factor L is not a sensitive parameter and it is normally kept fixed to 0.5. Similarly, θ_r does not affect the goodness-of-fit of the characteristic curve and it is typically eliminated [e.g., *Russo*, 1988; *Luckner et al.*, 1989; *Tietje and Tapkenhinchs*, 1993; *Boufadel et al.*, 1998; *Schaap and Leij*, 1998; *Ines and Droogers*, 2002]. Hence, in this study, θ_s , h_{ae} , n , and K_s are the sole hydraulic parameters to be inverted. The expected range of the above parameters is provided in Table 1; this range was computed by taking the 90% confidence interval of the combined datasets of GRIZZLY [Haverkamp et al., 2005] and UNSODA [Leij et al., 1996]. In particular, the minimum range of θ_s is determined for each hydroclimate by calculating the maximum range of the reference θ .

2.1.2. Modified Sink Term of SWAP 3.2 (SWAP_{inv})

[18] Building parsimonious SWAP models by reducing the number of input vegetation parameters, without decreasing their predictive capacity and their physical concept, are a challenging task. In this context, we modified the evaporation, transpiration, and rainfall interception modules of SWAP, next termed SWAP_{inv}, in order to use a reduced number of input parameters, namely the Leaf Area Index (LAI), the extinction coefficient of solar radiation (K_g), the rooting depth, and the saturated (θ_s) and residual (θ_r) water contents. In this respect, we use the Beer-Lambert law that partitions potential evaporation, potential

transpiration, and potential evaporation of a wet canopy by using LAI and K_g [e.g., *Ritchie*, 1972; *Goudriaan*, 1977; *Belmans et al.*, 1983]. In addition, LAI, K_g , and the potential evaporation of a wet canopy are also used to compute the interception, based on the works of *Noilhan and Lacarriere* [1995] and *Varado et al.* [2006]. Thus, the sensitivity of LAI and K_g is increased since they control multiple processes. The modified SWAP evaporation module does not require extra parameters, since it is directly estimated from the soil moisture, the potential soil evaporation, and the hydraulic parameters [e.g., *Eagleson*, 1978; *Milly*, 1986; *Simmons and Meyer*, 2000; *Romano and Giudici*, 2007, 2009]. Consequently, the sharing of the hydraulic parameters, which computes soil moisture and evaporation, increases the sensitivity of the hydraulic parameters when they are inverted simultaneously from soil moisture and evapotranspiration. The general shape of the roots in SWAP is entered manually in tabular form. Nevertheless, for large-scale modeling, a detailed description of roots is not required, thus we introduced an empirical power-law root density function [Gale and Grigal, 1987], that was further modified by *Pollacco et al.* [2008a]. The root density function requires two parameters, the maximum rooting depths and the percentage of roots in the top 30 cm. A detailed mathematical description of SWAP_{inv} is provided in Appendix A.

2.2. Generation of Reference Data for Numerical Experiments

[19] The numerical experiments were carried out for 22 hydroclimatic scenarios, derived by combining three soil types, two rooting depths, and five climates (Table 2). In order to provide realistic simulations, deep roots (DR) were not assigned to subtropical climates and shallow roots (SR) were not allocated to arid climate [Schenk and Jackson, 2002]. Moreover, in semiarid climates, only loamy sand was modeled. More precisely:

[20] 1. The hydraulic parameters for the three contrasting benchmark soils (loamy sand, silty loam, and silty clay) are given in Table 3. These soil textures were selected from *Carsel and Parrish* [1988] and *Ines and Mohanty* [2008b], and they ensure a large variability of annual evapotranspiration and groundwater recharge.

[21] 2. For the two contrasting benchmark-rooting depths (i.e., shallow and deep), the rooting depths and the percentage of roots for the top 30 cm are given in Table 4. These contrasting rooting depths were selected to depict shrubs, and they are provided by *Schenk and Jackson* [2002] and *Jackson et al.* [1996]. Forested land use was not selected, because remote sensing platforms using passive microwave still cannot retrieve soil moisture under dense canopy, the biomass of which is higher than 8 kg m^{-2} (e.g., vegetation denser than mature corn) [e.g., *Jackson and Schmugge*, 1991; *Bindlish et al.*, 2006; *Li et al.*, 2006; *Njoku and Chan*, 2006].

[22] 3. The values of the typical vegetation parameters that remain constant for all simulations are provided in Table 5 and explained in Appendix A. It is assumed that all these parameters can be retrieved from MODIS remote sensing [e.g., *Huete et al.*, 2002; *Simic et al.*, 2004; *Nagler et al.*, 2005; *Vegas Galdos et al.*, 2012].

[23] 4. To formulate the hydroclimatic scenarios, we used daily precipitation time series and meteorological data for

Table 1. Expected Parameter Space of the van Genuchten Hydraulic Parameters Computed by Taking the 90% Confidence Interval of the Combined Data Sets of GRIZZLY [Haverkamp et al., 2005] and UNSODA [Leij et al., 1996]^a

| | θ_s ($m^3 m^{-3}$) | h_{ae} (cm) | n (-) | K_s ($cm d^{-1}$) |
|---------|-----------------------------|---------------|---------|-----------------------|
| Minimum | MAX(θ_{ref}) | 7.6 | 1.09 | 0.48 |
| Maximum | 0.54 | 375 | 2.3 | 465 |

^aThe minimum range of θ_s is computed from the maximum value of reference θ .

Table 2. Contrasting 22 Scenarios Composed of Three Soil Types, Two Rooting Depths, and Five Climates^a

| | | Temp. Arid | Semi-Mediter. | Temp. Continental | Temperate | Subtropical |
|---------------|------------|------------|---------------|-------------------|-----------|-------------|
| Shallow roots | Loamy Sand | | ✓ | ✓ | ✓ | ✓ |
| | Silt Loam | | ✓ | ✓ | ✓ | ✓ |
| | Silty Clay | | ✓ | ✓ | ✓ | ✓ |
| Deep roots | Loamy Sand | ✓ | ✓ | ✓ | ✓ | |
| | Silty Loam | | ✓ | ✓ | ✓ | |
| | Silty Clay | | ✓ | ✓ | ✓ | |

^aTo maintain the simulations more realistic deep roots were not assigned to subtropical climates and shallow roots were not allocated to arid climate.

computing the potential evapotranspiration through the *Penman and Monteith* formula [1965], which were compiled from AmeriFlux <http://public.ornl.gov/ameriflux/> (Table 6). The contrasting climates correspond to typical mainland Southern United States conditions, for which snowfall is scarce. The forcing data was selected by combining a dry, a normal, and a wet water year (1 October to 30 September).

[24] A summary of the 22 reference water fluxes computed with SWAP_{inv} is presented in Figure 2. The scenarios provide satisfactory high variability of the model fluxes. Specifically, the annual groundwater recharge ranges from 30 to 800 mm, the annual transpiration ranges from 120 to 370 mm, and the annual evaporation ranges from 7 to 144 mm.

2.3. Boundary Conditions and Discretization

[25] Within the simulations, the soil column was discretized for deep roots of a total depth of 1.80 m and for shallow roots of a total depth of 0.90 m. Finer discretization (0.25 cm) near the land atmospheric boundary and coarser discretization (5 cm) at deeper depths were employed. For all scenarios, the soil columns were initialized uniformly at $h = -0.1$ m and SWAP_{inv} run for 90 days (spin up time) ahead of the experiment, to tune the state of the initial soil moisture profile. For the bottom boundary condition of the soil columns, the free drainage was selected. The upper boundary condition was determined by the daily net precipitation, which was computed with the interception model, and the potential evapotranspiration, estimated by the Penman-Monteith equation. The potential evapotranspiration was partitioned into potential soil evaporation, potential evaporation of wet canopy, and potential transpiration by using the Beer-Lambert law [e.g., *Ritchie*, 1972; *Goudriaan*, 1977; *Belmans et al.*, 1983]. Finally, a maximum of 2 cm of ponding water is permitted with any overflow lost as runoff.

2.4. Formulation of the Inverse Problem

2.4.1. The Weighted Objective Function

[26] Within the inverse problem, we use a WOF comprising two fitting criteria, OF_θ and OF_{et} , and two control variables, w and θ_d . In order to account for the differences in magnitude between the individual criteria, it is preferable that all the components of the WOF are either dimensionless or normalized. The WOF is derived by dividing the mean absolute error by the typical observation error

(uncertainty) of the corresponding reference state or flux, i.e.,

$$OF_\theta = \frac{\sum_1^{N_\theta} |\theta_{ref} - \theta_{sim}|}{N_\theta \Delta\theta_{rs}} \quad \text{and} \quad OF_{et} = \frac{\sum_1^{N_{et}} |ET_{ref} - ET_{sim}|}{N_{et} \Delta ET_{rs}} \quad (5)$$

where θ [$L^3 L^{-3}$] is the top 5 cm surface soil moisture where decoupling does not occur and N_θ and N_{et} are the lengths of daily soil moisture and evapotranspiration time series, respectively. When OF_θ or OF_{et} is greater than 1 indicates that the errors of simulations are greater than the uncertainties of retrieving the observation from remote sensing. We highlight that for both functions, all model outputs which provide values greater than 1 are considered as nonacceptable. Hence, a trial set is rejected if $OF_\theta > 1$ or $OF_{et} > 1$.

[27] To provide a proper configuration of the multiobjective calibration problem, it is essential to ensure that the two fitting criteria, OF_θ and OF_{et} , are approximately uncorrelated. Indeed, *Pollacco and Mohanty* [2012] showed that for contrasting hydroclimatic conditions the related processes θ and ET are rather independent. This is because the surface θ is influenced by the evaporation and decouples between the surface and root-zone soil moisture, while ET is a signature of the whole root-zone θ , since ET results in the uptakes of water stored at depth. In addition, the storage of θ in the root-zone profile is dependent on the past weather events, whereas the near-surface θ reflects the present weather condition.

2.4.2. Introducing Decoupling Within WOF

[28] One of the peculiarities when calibrating hydrological models against surface soil moisture is that soil moisture is prone to decoupling. This originates from the significantly faster drying of the surface compared to the root zone, due to evaporation and shallow root water uptake, causing a sharp vertical soil water gradient near the surface. When this occurs, the surface θ is no more representative of the soil moisture dynamics in the rooting zone [*Capenhart and Carlson*, 1997; *Walker et al.*, 2002; *De Lannoy et al.*, 2007; *Pollacco and Mohanty*, 2012]. For instance, large-scale decoupling was evidenced in New Zealand by *Wilson et al.* [2003] between 0–6 cm and 0–30

Table 3. Reference Values of the *Mualem* [1976] and *van Genuchten* [1980] Hydraulic Parameters

| Texture | Acronym | θ_s ($m^3 m^{-3}$) | θ_r ($m^3 m^{-3}$) | L (–) | h_{ae} (cm) | n (–) | K_s ($cm d^{-1}$) | Sources |
|------------|---------|-----------------------------|-----------------------------|---------|---------------|---------|-----------------------|----------------------------------|
| Loamy sand | LS | 0.41 | 0.057 | 0.5 | 8 | 2.28 | 350.2 | <i>Carsel and Parrish</i> [1988] |
| Silty loam | SiL | 0.43 | 0.061 | 0.5 | 83 | 1.39 | 30.5 | <i>Ines and Mohanty</i> [2008b] |
| Silty clay | SiC | 0.36 | 0.07 | 0.5 | 200 | 1.09 | 0.48 | <i>Carsel and Parrish</i> [1988] |

Table 4. Contrasting Scenarios of the Percentage of Roots in the Top 30 cm, ΔRDF_{30} [Jackson et al., 1996], and Maximum Rooting Depths, z_{root} [Schenk and Jackson, 2002]

| Description | Acronym | z_{root} (cm) | ΔRDF_{30} (%) | Vegetation Type |
|---------------|---------|------------------------|-----------------------------|-----------------|
| Shallow roots | SR | 40 | 80 | Meadows |
| Deep roots | DR | 130 | 50 | Semidesert |

cm in situ. Decoupling is more prominent when surface θ is in the drying phase and it is below the threshold θ_d ($\text{L}^3 \text{L}^{-3}$), which is computed by

$$\theta_{\text{ref}}(t) < \theta_d \text{ and } \theta_{\text{ref}}(t+1) < \theta_{\text{ref}}(t) \quad (6)$$

[29] On the basis of equation (6), we modified OF_θ such that to increase its sensitivity by omitting the period when surface and root-zone decoupling occurs. If $\theta_d = 0$, decoupling is not taken into account within WOF.

3. Outline of the Weighted Objective Function Selector Algorithm (WOFSA)

3.1. Identification of the Best-Compromise Parameter Set in Multiobjective Calibration: Approaches and Drawbacks

[30] Equation (1) is a specific case of aggregated objective functions that represent an overall measure of the model performance, in which the characteristics of the best-compromise solution, which also reflect the relative importance of the individual criteria, are specified a priori. The later are expressed in terms of multipliers (e.g., weighting method), target values combined with distance metrics (e.g., goal programming and ε -constraint methods) [e.g., Laumanns et al., 2002; Reed et al., 2003] or priorities (e.g., lexicographic ordering). Besides, the detection of the best-compromise parameter set remains an open issue in hydrological calibration, which has not been thoroughly addressed in the literature [e.g., Dumedah et al., 2010].

[31] Most approaches employ hybrid strategies, based on combined objective and subjective criteria, to support the manual identification of the “most prominent” parameter values [e.g., Efstratiadis and Koutsoyiannis, 2010]. In particular, a well-accepted technique for detecting the best-compromise parameters, which is usually employed in subsurface flow modes, is by minimizing the Euclidean distance of the Pareto set to the origin [e.g., Refsgaard and Storm, 1996; Madsen, 2003; Twarakavi et al., 2008]. Although this methodology, which is a subcase of goal programming, appears to be statistically reasonable, its hydrological meaning is not well understood. On the other hand,

few are the procedures for recognizing effective nondominated solutions a posteriori, through systematic filtering of the Pareto set. Some of the proposed approaches are preference ordering and compensation between model objectives [e.g., Khu and Madsen, 2005] as well as cluster analysis [e.g., Taboada and Coit, 2006; Crispim and de Sousa, 2009; Dumedah et al., 2010]. For instance, Dumedah et al. [2010, 2012a, 2012b] used cluster analysis to evaluate the distribution of solutions on the trade-off surface, to find relationships in both objective space and parameter space. The linkage between the two spaces describes the level of robustness for the parameter sets (according to Deb and Gupta [2005], robust solutions are less sensitive to variable perturbations in their vicinity). They also showed that the use of criteria that are based on a compromise between representative pathways in the parameter space and a dominant variability in the objective space provides solutions that remain nondominated across different validation subsets.

[32] The above, rather subjective, approaches for detecting the best-compromise parameter set in multiobjective calibration problems, ignore uncertainties that are due to errors in input data, which prevent providing robust solutions. In this respect, we are proposing a systematic procedure, called weighted objective function selector algorithm (WOFSA), which identifies the most appropriate weighted objective function (WOF), by performing inverse modeling, where the uncertainties in retrieving θ and ET data are directly accounted for. Next are described the key assumptions of the methodology as well as the detailed computational procedure.

3.2. Key Assumptions of WOFSA

[33] The key idea of WOFSA is based on the postulation that the optimal weighting between the individual objectives is the one ensuring the maximum linear correlation between the residuals ΔWF of the computed model responses of interest (water fluxes) and the WOF. The rationality is that if the inverse modeling is well posed, then an increase in the OF should cause the error of each specific simulated flux to also increase and vice versa [Pollacco et al., 2008a]. If the later is insensitive against to variations of θ and ET , the problem is ill-posed as the modeled flux cannot be calibrated solely from the observed θ and ET ; thus, additional observations should be included into the WOF.

[34] This assumption is further illustrated in Figure 3, where we plot three hypothetical relationships between a normalized WOF* and a dimensionless residual metric (e.g., relative bias) ΔQ^* , which is a measure of uncertainty of the corresponding water flux (in the specific case, the groundwater recharge). It is assumed that the optimal

Table 5. Values of Vegetation Parameters that Remains Constant, Where h_1 , h_2 , $h_{3\text{high}}$, $h_{3\text{low}}$, and h_4 are the Capillary Pressure Head that Regulate the Water Uptake Model, LAI is the Leaf Area Index, β is the Crop Factor, and K_g is the Extinction Coefficient of Solar Radiation (–)^a

| h_1 (cm) | h_2 (cm) | $h_{3\text{high}}$ (cm) | $h_{3\text{low}}$ (cm) | h_4 (cm) | LAI ($\text{m}^2 \text{m}^{-2}$) | K_g (–) | β (–) |
|----------------------|------------|-------------------------|------------------------|------------|------------------------------------|-----------------------|------------------|
| –1 | –22 | –1000 | –2200 | –16,000 | 2 | 0.5 | 0.9 |
| [Singh et al., 2006] | | | | | [Brutsaert, 2005] | [Varado et al., 2006] | [Pollacco, 2005] |
| Wheat | | | | | Scrubland | Universal | Grassland |

^aRefer to Appendix A for further information.

Table 6. Sources of Reference Hydroclimate Data Compiled From AmeriFlux (<http://public.ornl.gov/ameriflux/>)

| Climate | Acronym | Site | State | Lat. | Long. | IGBP Classif. |
|--------------------|---------|--------------------------------|-------|------|-------|-------------------|
| Temperate semiarid | Tsa | Kendall Grassland | AZ | 32 | -110 | Grasslands |
| Mediterranean | M | Tonzi Ranch | CA | 38 | -121 | Woody Savannas |
| Temp. continental | Tc | Walnut river | OK | 37 | -97 | Cropland |
| Temperate | T | Mead Rainfed | NE | 41 | -96 | Croplands |
| Subtropical | S | Kennedy Space Center Scrub Oak | FL | 29 | -81 | Closed shrublands |

relationship is the 1:1 line (intermediate curve of Figure 3, e.g., 2), which indicates that a specific change of the WOF^{*} value results to an equal change of the model uncertainty ΔQ^* . Therefore, this expression is the most suitable to be used in calibration. Any other relationship, derived by different combinations of weights, is suboptimal. For instance, the right curve of Figure 3 (e.g., 1) demonstrates a weighted function that initially has limited sensitivity against the model uncertainty (a significant change of the WOF^{*} results to a much less significant change of ΔQ^*), followed by sharply varying model uncertainty for small changes of the WOF^{*}. On the other hand, the left curve of Figure 3 (e.g., 3) represents an opposite performance, which is also far from desirable. This feature forms the basis for our linearity assumption between WOF^{*} and ΔQ^* in WOFSA.

3.3. Description of Computational Procedures

[35] The algorithm is applied to a SWAP_{inv} model, using the objective functions of section 2.4. The model runs on daily basis. The water fluxes of interest are groundwater recharge Q (mm d⁻¹), evaporation E (mm d⁻¹), transpiration T (mm d⁻¹), evapotranspiration ET (mm d⁻¹), while the modeled state variables are the root-zone soil moisture θ_{rz} (m³ m⁻³) and the surface soil moisture θ (m³ m⁻³). The method is performed in three successive steps, as also shown in the flowchart of Figure 4

3.3.1. Step 1: Generation of Reference Runs

[36] WOFSA performs numerical experiments to determine the optimal control variables w and θ_d of the WOF, which requires that the soil moisture θ , evapotranspiration

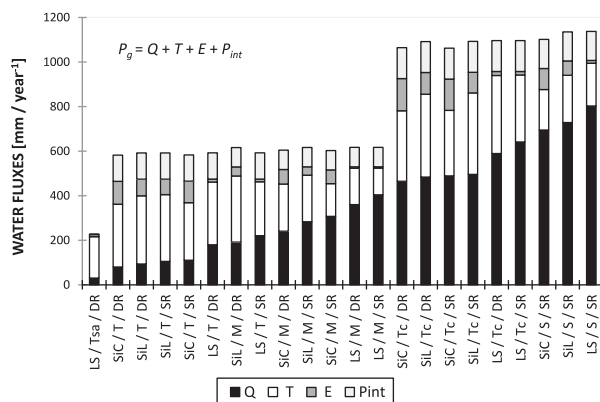


Figure 2. The 22 hydroclimatic scenarios depicted by average yearly groundwater recharge Q , transpiration T , evaporation E , interception P_{int} computed from SWAP_{inv}. For visualization, the gross precipitation $P_g = Q + T + E + P_{int}$ with the long-term storage computed to 0. The acronyms are provided in Table 3 for the soil texture, in Table 4 for the roots, and in Table 6 for the climate.

ET , and water fluxes (as well as state variables) WF, are known a priori. The later will be next called “reference” data, symbolized θ_{ref} , ET_{ref} , and WF_{ref} , respectively. In particular, WF_{ref} are computed by inputting known sets of hydraulic parameters (HYDRAU_{ref}), vegetation parameters (VEGETATION_{ref}), and daily forcing (precipitation, potential evapotranspiration) data into SWAP_{inv} (Figure 4, Loop 1). We remark that the vegetation parameters are treated as known properties of the model (cf. section 2.2), while the soil hydraulic parameters are to be inverted through optimization.

3.3.2. Step 2: Monte Carlo Simulation and Calculation of Uncertainties

[37] In order to assess the uncertainties in retrieving θ_{ref} and ET_{ref} from remote sensing, we use different sets of θ_{sim} and ET_{sim} provided through Monte Carlo simulation (Figure 4, Loop 2). Each trial set is formulated on the basis of different values of soil hydraulic parameters (HYDRAU_{sim}), which are generated by SWAP_{inv} to provide the corresponding simulated time series WF_{sim} , θ_{sim} , and ET_{sim} . The “unknown” constrained HYDRAU_{sim} are estimated by minimizing the WOF. To initialize the search procedure, the typical values $w = 0.5$ and $\theta_d = 0$ are assigned to WOF, which are updated after the completion of Step 3. The simulations are carried out by employing the Shuffled Complex Evolution University of Arizona (SCE-UA) algorithm, developed by Duan *et al.* [1992, 1994]. The customized global optimization can be seen as a restrained Monte Carlo simulation that seeks for different combinations of “compromise” parameter sets (HYDRAU_{sim}), in the vicinity of

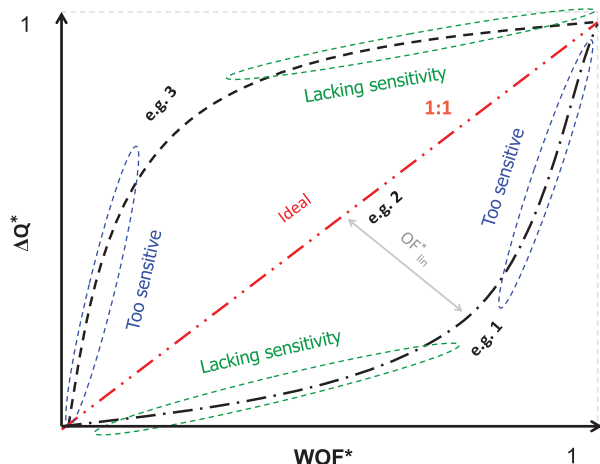


Figure 3. Examples of relationship between a normalized weighted objective function (WOF^{*}) with the normalized uncertainty of the water flux (ΔQ^*) error represented by ΔQ^* . The ideal is a linear correlation between WOF^{*} and ΔQ^* .

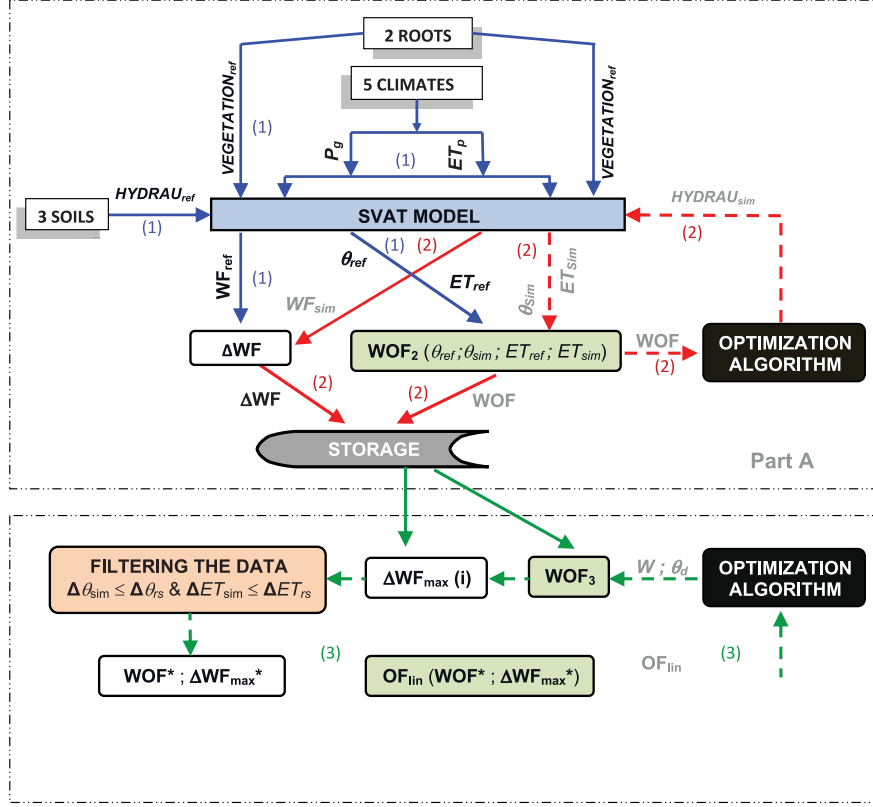


Figure 4. Flowchart of the weighted objective function selector algorithm (WOFSA) where $HYDRAU_{ref}$ and $VEGETATION_{ref}$ are a known set of reference parameter values; WF_{ref} are the modeled reference water fluxes outputs that are computed from the SVAT hydrological model requiring a priori known sets of hydraulic parameters ($HYDRAU_{ref}$) and gross precipitation (P_g) and potential evapotranspiration (ET_p) as forcing data; $HYDRAU_{sim}$ are the trial set of parameter values that are obtained from the OPTIMIZATION ALGORITHM; WF_{sim} are the simulated fluxes and ΔWF is their residuals, derived by a posteriori estimated hydraulic parameters ($HYDRAU_{sim}$) by minimizing the weight w (between the fitting criteria based on soil moisture θ and evapotranspiration ET) and the decoupling threshold θ_d of WOF. All the trials are stored in the STORAGE and are filtered such that the uncertainties in θ_{sim} and ET_{sim} are not greater than the uncertainties of retrieving θ and ET from remote sensing ($\Delta\theta_{rs}$ and ΔET_{rs}). WOFSA is performed in two separate parts: Part A generates uncertainties in the fluxes ΔWF as if they were available from independent measurements, while Part B optimizes w and θ_d by minimizing the OF_{lin} such that to ensure the maximum linearity between the normalized WOF* and the normalized maximum uncertainty ΔWF_{max}^* . The different loops are colored coded with blue for loop 1, red for loop 2, and green for loop 3.

the global minimum [van Griensven and Meixner, 2006; Pollacco et al., 2008a, 2008b].

[38] For each trial set (i.e., hydraulic parameters and resulting fluxes), the model uncertainties, in terms of residuals ΔWF , are computed by

$$\Delta WF = \frac{\sum_{t=1}^{t=N_{wf}} |WF_{ref}(t) - WF_{sim}(t)|}{\sum_{t=1}^{t=N_{wf}} WF_{ref}(t)} \quad (7)$$

where N_{wf} is the time length of simulations (days).

[39] During the Monte Carlo procedure, all the different trials of $HYDRAU_{sim}$ and the corresponding WF_{sim} and ΔWF are stored in the STORAGE archive (Figure 4). At the end of Step 2, the trial sets are sorted in increasing order of WOF values. Figure 5a depicts the relationship between

WOF and the residuals of the groundwater recharge ΔQ , for one of the experiments that are examined next (i.e., loamy sand, temperate climate, and short rooting depth).

3.3.3. Step 3: Estimation of w and θ_d

[40] As explained in section 3.2, in order to determine the best-compromise values of w and θ_d , it is essential to ensure the greatest linearity between the so-called normalized WOF and the normalized maximum uncertainties ΔWF_{max}^* . This linearity is obtained by minimizing an “auxiliary” objective function OF_{lin} through the SCE-UA method, using the ensemble sets that are generated in Step 2. The computational procedure is the following.

[41] From each generated WOF_i , the maximum corresponding error of WF_{sim} (ΔWF_{max}) is selected and plotted. As shown in Figure 5b (where ΔWF_{max} is ΔQ_{max}), the key assumption is that the relationship between WOF and

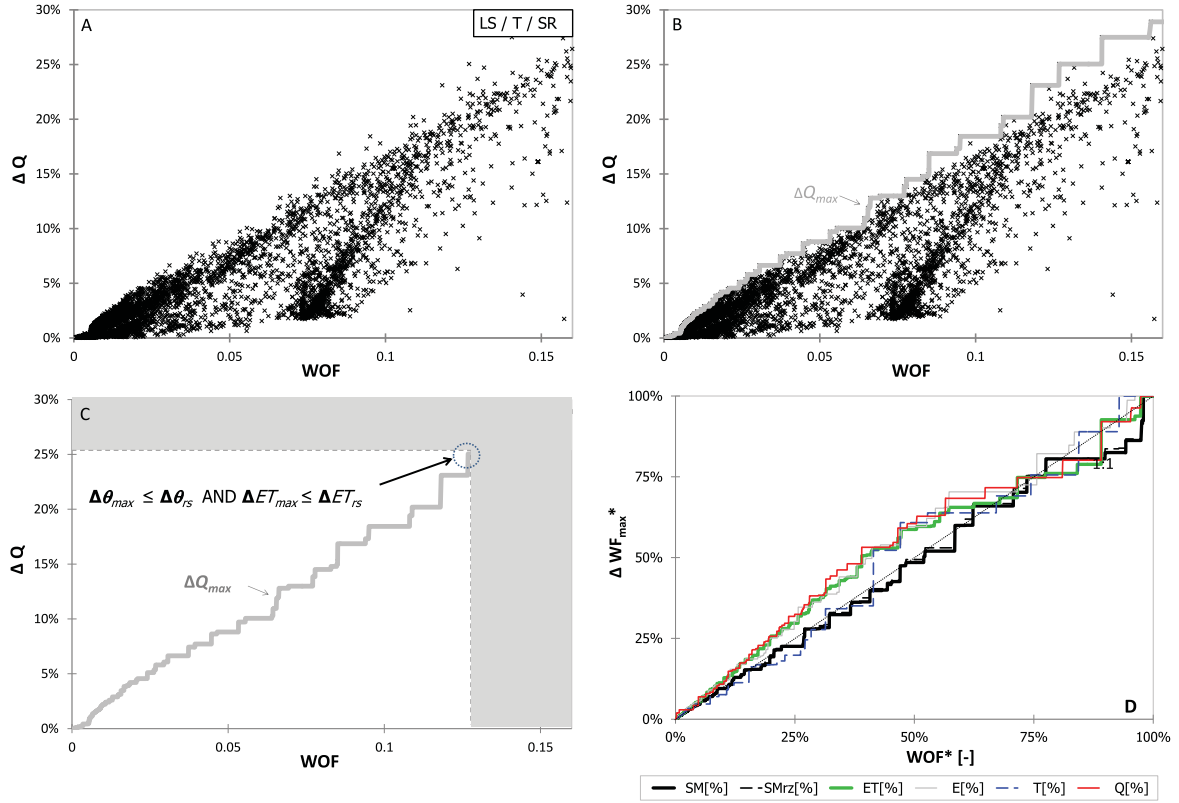


Figure 5. Different steps of the WOFSA given as an example for loamy sand, temperate climate, and short rooting depth. (a) An ensemble of generated parameter sets $HYDRAU_{sim}$ with the relationship between WOF and the residuals between reference and simulated WF_{sim} given as an example for ground-water recharge ΔQ . (b) From each generated WOF_i , described in Figure 5a, the maximum corresponding error ΔQ_{max} is selected. (c) Selection of feasible parameter sets ΔQ_{max} to reproduce the uncertainties in retrieving θ_{ref} and ET_{ref} from remote sensing. (d) Correlation between normalized WOF^* and normalized ΔWF_{max}^* for top soil moisture SM (θ), root-zone soil moisture SM_{rz} (θ_{rz}) evapotranspiration ET , evaporation E , transpiration T , and groundwater recharge Q .

ΔWF_{max} monotonically increases is reasonable. The computation of ΔWF_{max} is mathematically expressed as

$$\Delta WF_{max}(i+1) = \max \{ \Delta WF(i+1), \Delta WF(i) \} \quad (8)$$

$$\text{and } \Delta WF_{max}(i+1) \geq \Delta WF_{max}(i)$$

where index i corresponds to the i^{th} simulation, classified by an increasing order of WOF. We remind that here we only consider the uncertainties of the reference data that are used in calibration, and we do not take into account other error sources, such as structural errors of the model. In order to implicitly account for the later, we use the upper envelope uncertainties of the water fluxes ΔWF_{max} and not, for instance, their average values.

[42] For each flux, in order to evaluate the linearity between WOF and ΔWF_{max} , the two variables are normalized, thus taking values in the range $[0, 1]$. This is performed by selecting the corresponding “envelopes” of simulated ΔWF_{max} such that the following condition is fulfilled

$$OF_{\theta} = \Delta \theta \leq \Delta \theta_{rs} \text{ and } OF_{et} = \Delta ET \leq \Delta ET_{rs} \quad (9)$$

where $\Delta \theta_{rs}$ and ΔET_{rs} are typical values of the uncertainties in retrieving θ and ET , respectively, from remote sensing.

In the case study, we generated 7000 sets of θ_{sim} and ET_{sim} which comply with equation (9). Preliminary investigations indicated that generating more sets improve the optimal values of w and θ_d only marginally. On the basis of literature data already mentioned in section 1, for the soil moisture we assigned a volumetric root-mean-square error $\Delta \theta_{rs} = 0.04 \text{ m}^3 \text{ m}^{-3}$ while for the evapotranspiration we set a relative error $\Delta ET_{rs} = 20\%$ (apparently, in a particular study, different values can be employed, taking advantage of uncertainty estimations based on local data). The simulated ΔWF_{max} values that comply with equation (9) are depicted in Figure 5c, through the nonshaded area. WOF and ΔWF_{max} are normalized and symbolized with (*), using the maximum feasible simulated value that complies with equation (9), which is annotated with the circle in Figure 5c.

[43] As explained in section 3.2, the optimal WOF is determined such that to ensure the maximum linearity between WOF^* and ΔWF_{max}^* . The linearity is quantified by means of the auxiliary objective function OF_{lin} (Figure 3), which is computed separately for each water flux, as follows:

$$OF_{lin}^* = \frac{\text{MAX} |\Delta WF_{max}^*(i) - WOF_i^*(w, \theta_d)|}{\sqrt{2}/2} \quad (10a)$$

where the index i corresponds to the i^{th} simulation, classified by an increasing order of ΔWF_{max}^* and $\sqrt{2}/2$ is only used for graphical reasons, i.e., in order to normalize OF_{lin} thus being equal to half the diagonal of a unit square.

[44] The value of OF_{lin}^* depicts the maximum deviation from the 1:1 line composed of ΔWF_{max}^* and WOF^* , as described in Figure 3. The value $OF_{lin} = 0$ denotes a perfect linearity, while $OF_{lin} = 1$ corresponds to the greatest deviation from the desirable line 1:1. The final value of OF_{lin} is computed by averaging OF_{lin}^* , which is calculated for each individual water flux and state variables of interest (root-zone soil moisture, groundwater recharge, evapotranspiration, evaporation, and transpiration) by using the following expression:

$$\overline{OF_{lin}^*} = \sqrt{\frac{\sum_1^{N_{OF_{lin}}} OF_{lin}^*(j)^2}{N_{OF_{lin}}}} \quad (10b)$$

where index j corresponds to j^{th} water flux of interest and $N_{OF_{lin}}$ is the number of water fluxes of interest. An example of the relationship between the optimal WOF^* and ΔWF_{max}^* for all water fluxes is provided in Figure 5d.

[45] The SCE-UA optimization algorithm is next used to minimize the auxiliary function (equation (10b)) against w and θ_d . After getting the optimal values of w and θ_d , the initial objective function (WOF) is updated and Steps 2 and 3 are repeated. The iterative procedure continues until the values of w and θ_d are stabilized, thus $WOF_i \approx WOF_{i-1}$. Typically, four runs are enough to achieve convergence.

4. Results

4.1. General Outcomes

[46] An overview of the WOFSA capabilities is provided by investigating the three representative scenarios, which are presented in Table 7 and plotted in Figure 6. The figure shows the relationship between WOF^* and ΔWF_{max}^* , which is computed for ET , T , E , θ , θ_{rz} , and Q . The following general outcomes are drawn:

[47] 1. The strength of linearity between WOF^* and ΔWF_{max}^* can vary greatly with hydroclimate conditions (Figure 6).

[48] 2. The usage of the decoupling algorithm (equation (6)) increases the linearity between WOF^* and ΔWF_{max}^* (e.g., for loamy sand; Figure 6a).

[49] 3. Deep roots compared to shallow roots tend to increase the discrepancy in the predictions of transpiration (e.g., for sandy clay; Figure 6b).

[50] 4. The usage of WOF instead of a single OF_{et} did not improve the linearity between WOF^* and ΔWF_{max}^* .

Table 7. Detailing the Different Scenarios Used in Figure 6

| Texture | Specification | OF_{lin} (%) | Figure 6 |
|------------|---------------------------|----------------|----------|
| Loamy sand | Decoupling equation | 21 | A1 |
| | No decoupling | 17 | A2 |
| Sandy clay | Shallow roots | 13 | B1 |
| | Deep roots | 10 | B2 |
| Silty clay | Calibrated with OF_{et} | 13.9 | C1 |
| | Calibrated with WOF | 14.5 | C2 |

(e.g., for silty clay under a Mediterranean climate for which we will show that it is a special case; Figure 6c).

[51] Next, we further investigate how the optimized values of w and θ_d vary under different hydroclimatic conditions.

4.2. Correlating Soil Moisture Decoupling With Hydroclimatic Variables

[52] The weighting coefficient w and the decoupling threshold θ_d ($\text{m}^3 \text{m}^{-3}$) were optimized by minimizing OF_{lin} (equation (10b)). As already mentioned in section 2.4.2, to account for the observed θ within WOF we only used periods when soil moisture decoupling does not occur. We remind that decoupling only occurs when the soil is drying and the soil moisture falls below θ_d . For loamy sands, an example of decoupling is given in Figure 7a, where the reference time series of soil moisture θ are plotted at different depths. Figure 7a suggests that during the drying period and when $\theta < \theta_d = 0.07 \text{ m}^3 \text{m}^{-3}$ (where $0.07 \text{ m}^3 \text{m}^{-3}$ is the optimal value obtained through the WOFSA, for the specific combination of soil texture and climate), the surface moisture is decoupled from root-zone moisture.

[53] For each hydroclimatic scenario, we employed preliminary simulations to express θ_d as function of average surface soil moisture $\bar{\theta}$, average evapotranspiration \overline{ET} and its standard deviation σ_{ET} (Figure 8). The scatter plots indicate a negative correlation between $\overline{ET}/\sigma_{ET}$ and $(\theta_d/\bar{\theta})^{1/3}$. The ratio $\overline{ET}/\sigma_{ET}$ is a climatic indicator which increases as the climate gets wetter, since there is a positive correlation ($r^2 = 0.70$) between $\overline{ET}/\sigma_{ET}$ and the evapotranspiration fraction $\overline{ET}/\overline{ET}_{pot}$ (\overline{ET}_f) (results not provided here). On the other hand, the ratio $(\theta_d/\bar{\theta})$ can be viewed as a normalized expression of θ_d , where $\bar{\theta}$ is representative of the soil texture, which is lower for coarse texture and higher for fine texture. To understand the correlation we rewrite θ_d model as

$$\theta_d = \bar{\theta} \left(2.28 - 0.86 \frac{\overline{ET}}{\sigma_{ET}} \right) \quad (11)$$

[54] From the above equation, it results that when the soil moisture storage $\bar{\theta}$ in the root zone increases, \overline{ET} also increases, which is reasonable. An increase in $\bar{\theta}$ also generates a decrease in soil moisture decoupling, which is represented by a decrease in θ_d . However, a high value of σ_{ET} indicates more pronounced periods of drying and wetting, which in turn produces an increase in soil moisture decoupling θ_d , due to differences in the soil moisture storage between the surface and the root zone. Figure 8 shows that for dry hydroclimates $\theta_d/\bar{\theta} > 1$, while for wetter hydroclimates $\theta_d/\bar{\theta} < 1$. Thus, $\overline{ET}/\sigma_{ET}$ is negatively correlated with $(\theta_d/\bar{\theta})^{1/3}$. The conclusion that soil moisture decoupling is more pronounced in drier climates is in line with the results of *Capenhart and Carlson* [1997].

4.3. Correlating Weighting Coefficient With Hydroclimatic Variables

[55] A major objective of this study is to relate the weighting coefficient w with easily obtainable predictors. The optimal value of w is a complex trade-off between the

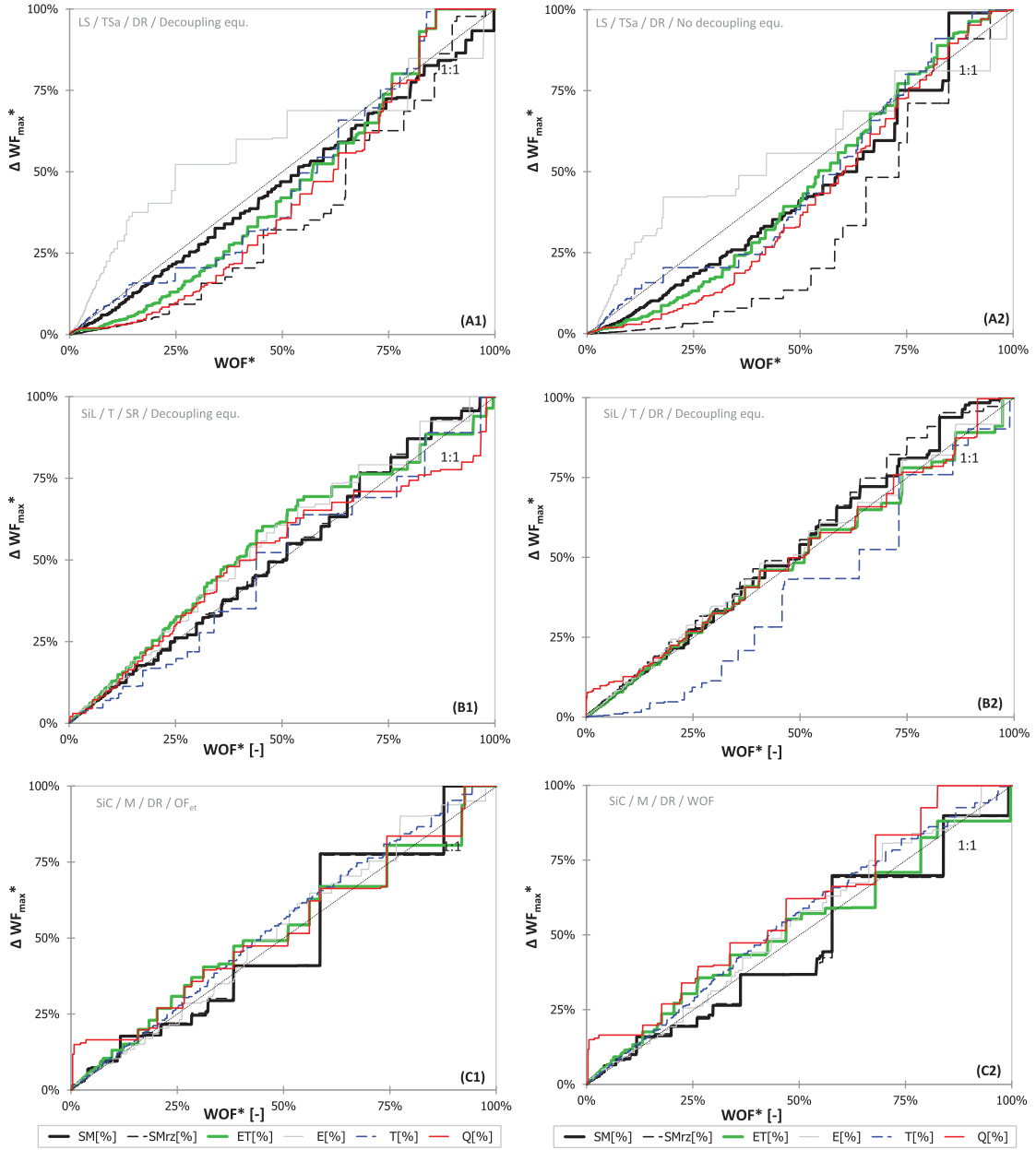


Figure 6. Relationships between normalized optimized WOF^* and normalized ΔWF_{max}^* for the scenarios described in Table 7.

information gathered by OF_θ and OF_{et} . When more weight is assigned to OF_θ , then the errors in $\Delta\theta_{rs}$ influences more the computation of the water fluxes (WF) compared to ΔET_{rs} . On the other hand, when more weight is assigned to OF_{et} then the errors in ΔET_{rs} influences more the computation of the WF compared to $\Delta\theta_{rs}$. In fact, the inverse modeling will favor the weighting to OF_θ , since θ is a better predictor of the hydraulic parameters than ET [Pollacco *et al.*, 2008a].

[56] For the three soil texture classes subdivided climatically, Figure 9a depicts the relationship of w against the average evapotranspiration fraction $\overline{ET}/\overline{ET}_{pot}$ and Figure 9b shows the correlation of w against the average measured surface soil moisture $\bar{\theta}$. For every texture class, the empirical linear equations of Figures 9a and 9b are described in Table

8. No correlation of the rooting depth with w was found since the former influences indirectly w through \overline{ET}_f . The hydroclimates that are enclosed in ovals are the ones for which little difference arises in OF_{lin}^* , given that OF_{et} is used instead of WOF. These hydroclimates are depicted by arrows, representing threshold values of $\bar{\theta}$ and ET_f .

4.3.1. Loamy Sand

[57] For coarser texture soils (loamy sand and sandy clay), w is negatively correlated to both \overline{ET}_f (Figure 9a) and $\bar{\theta}$ (Figure 9b). It is to be noted that $\bar{\theta}$ is small for coarse soils because, as shown in Figure 7a, there are long periods of droughts for which $\bar{\theta} \approx 0$. Therefore, for dry hydroclimates, represented by low values of \overline{ET}_f , more weight is assigned to OF_θ , and for wetter hydroclimates, represented by larger \overline{ET}_f , more weight is assigned to OF_{et} .

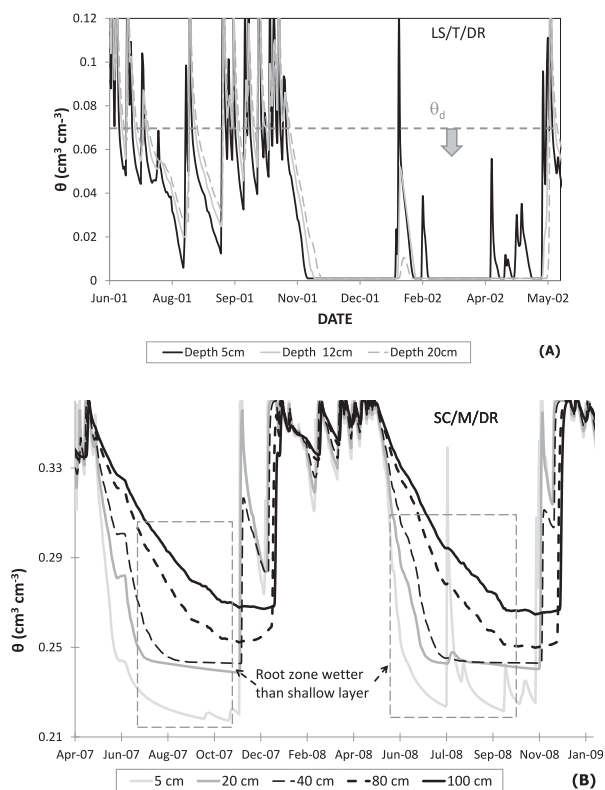


Figure 7. Reference time series θ plotted at different depths: (a) for coarse soils, showing that the top layer is decoupled from the deeper layer when θ is drying and $\theta < \theta_d$ and (b) for fine texture soils under dry climate, showing that the top layer gets gradually decoupled from the deeper layer.

[58] These results can be explained in terms of the sensitivity of OF_{et} against ΔWF , which depends on \overline{ET}_f . The later is computed from the water uptake function of Feddes *et al.* [1978], as shown in Figure 9c. The sensitivity of OF_{et} is considerably reduced when the vegetation is under arid conditions, with \overline{ET}_f as low as 10%. This is due to the closure of the stomata, thus more weight is assigned to

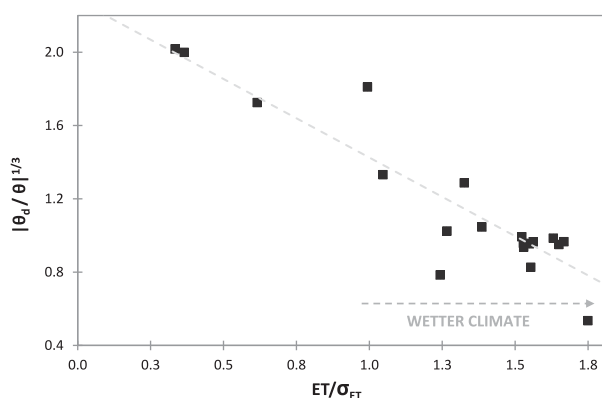


Figure 8. For all hydroclimatic conditions a relationship is obtained between average ET divided by the standard deviation of ET (σ_{ET}) with $(\theta_d / \theta)^{0.3}$. The scenarios are wetter as ET / σ_{ET} increases.

OF_θ . For wetter hydroclimatic scenarios characterized by an increase of \overline{ET}_f , the sensitivity of OF_{et} increases but at the same time OF_θ weakens due to the enhanced surface and root-zone decoupling caused by evaporation. As \overline{ET}_f further increases (hydroclimates enclosed in ovals in Figures 9a and 9b), OF_{lin}^* remains invariant if either OF_{et} or WOF is used independently. Therefore, under these hydroclimatic conditions, it is preferable to use OF_{et} instead of WOF. OF_{lin} remains invariant when $\overline{ET}_f > 68\%$ and $\theta > 0.035 \text{ L}^3 \text{ L}^{-3}$, approximately (refer to arrows in Figures 9a and 9b), where the relationships between w versus \overline{ET}_f and w against θ change slope. These outcomes explain why Ines and Droogers [2002], Ines and Mohanty [2008b], and Jhorar *et al.* [2002, 2004] did not find advantages of using a WOF instead of a single OF to optimize the hydraulic parameters.

4.3.2. Sandy Clay

[59] The behavior of sandy clay soils is very similar to the loamy sands described above. Nevertheless, sandy clays are less coarse than loamy sand and thus the average drainage and the evaporation rate is moderated. Therefore, for the nonarid hydroclimatic scenarios ($\overline{ET}_f > 70\%$), w is clustered around 0.60.

4.3.3. Silty Clay

[60] For finer texture soils (silty clay), w is positively correlated with both \overline{ET}_f (Figure 9a) and $\bar{\theta}$ (Figure 9b). Therefore, for dry hydroclimates more weight is assigned to OF_{et} and for wetter hydroclimates more weight is given to OF_θ . The correlation between w with $\bar{\theta}$ and w with \overline{ET}_f of fine texture soils is positive, while for coarse texture soils it is negative (Table 8). This difference arises because the vegetation under moist soils do not experience much stress, thus ET_f remains close to unity (Figure 9c). Under this premise, h is free to vary between h_2 and h_3 (equation (A8)), which reduces the sensitivity of OF_{er} . Thus, for wet hydroclimates, more weight is assigned to OF_θ .

[61] On the other hand, for drier hydroclimates, more weight is assigned to OF_{et} due to another type of decoupling, which occurs for fine texture soils termed as *fine texture decoupling*. An example is provided in Figure 7b, where the reference time series θ are plotted at different depths. Figure 7b suggests that for drier climates the top soil dries up progressively and decouples with the root zone, for which there is a substantial amount of water stored at depth. Under these conditions, ET is more representative of the root-zone soil moisture than the surface soil moisture, thus more weight should be assigned to OF_{et} .

5. Discussion

5.1. Selection of the Most Suitable Calibration Period

[62] It is widely accepted that the information which is embedded in calibration data plays much more important role than the length of observations themselves. However, most of the existing hydrological calibration approaches do not provide any guidance about which sets of measurements are most informative for specific model parameters [e.g., Vrugt *et al.*, 2002]. In particular, for SVAT models, an additional quest is to determine the “optimal” period to calibrate the hydraulic parameters from reference surface θ and ET retrieved from remote sensing. The use of a

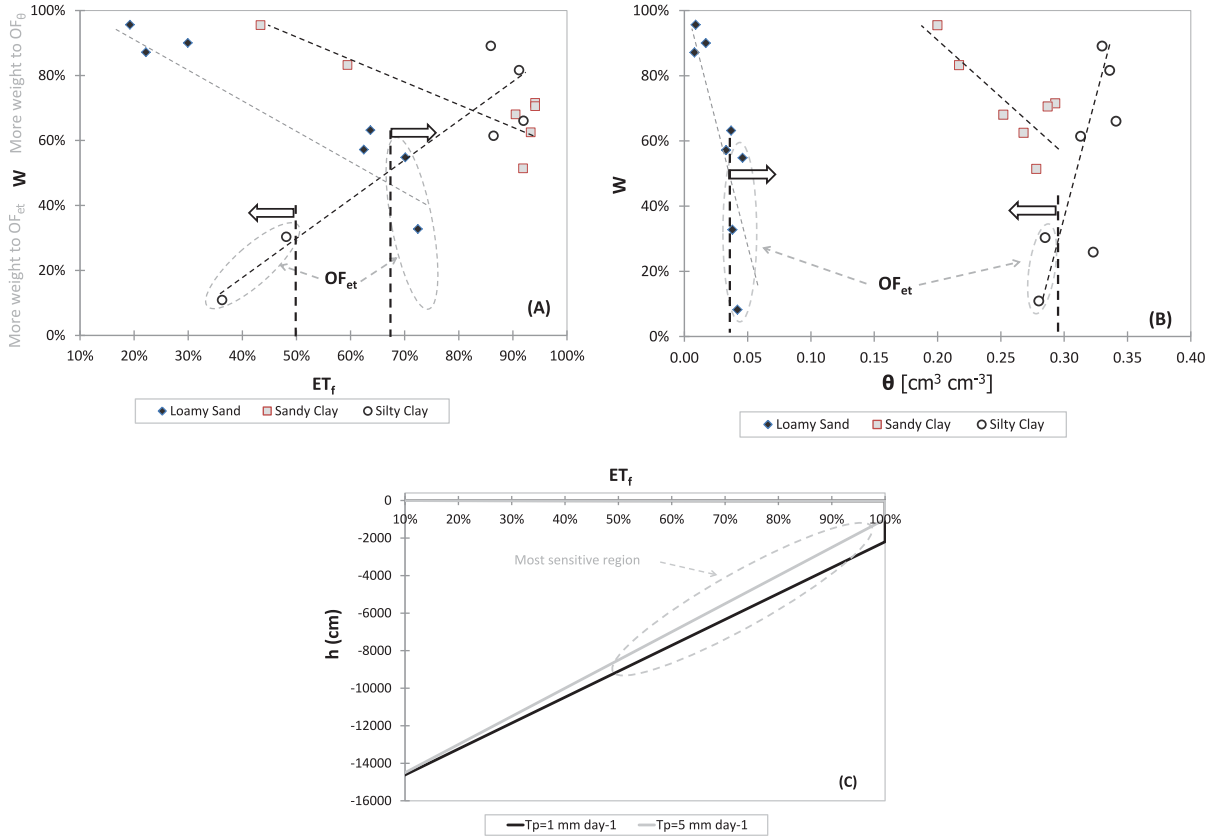


Figure 9. For the three soil textures class subdivided climatically: (a) relationship of w with average evaporative fraction ET_f , and (b) correlation of optimal w with the measured average θ . The empirical linear equations of each texture classes are described in Table 8. The enclosed hydroclimates are those for which a single OF_{et} can be used instead of a WOF. These hydroclimates are depicted by arrows which represent threshold values of θ and ET_f . Figure 9c schematizes the *Feddes et al.* [1978] plant water stress response function (ET_f) as a function of soil water pressure. The position of the parameter h_3 depends on the intensity of the potential transpiration ($T_p < 1 \text{ mm d}^{-1}$ or $T_p \geq 5 \text{ mm d}^{-1}$). The interpolation of h_3 is between the interval h_{3low} , h_{3high} for which their values are provided in Table 5.

multiobjective function, by means of the WOF, can adequately represent the errors that may be incurred due to the inverted parameter sets and may also help to recognize the structural errors much easier than when using a single fitting criterion. Therefore, to reduce ΔWF we need to select the period where the optimal w is theoretically around 0.6 (more weight is assigned to OF_θ , since θ is a better predictor of the hydraulic parameters), thus taking full advantage of the information provided simultaneously from OF_{et} and OF_θ .

[63] *Feddes et al.* [1993], *Ines and Mohanty* [2008c], *Jhorar et al.* [2002], and *Van Dam* [2000] suggested that

Table 8. Empirical Relationship for the Three Texture Classes Which Relates w With Average ET_f (ET/ET_p) and w With Average θ

| Texture | $w =$ | |
|------------|-------------------------------|----------------------------------|
| | Figure 10a | Figure 10b |
| Loamy sand | $-0.91\overline{ET_f} + 1.31$ | $-13.06\overline{\theta} + 1.04$ |
| Sandy clay | $-0.59\overline{ET_f} + 1.20$ | $-3.10\overline{\theta} + 1.5$ |
| Silty clay | $1.15\overline{ET_f} - 0.28$ | $9.63\overline{\theta} + 2.52$ |

the identifiability of the parameters increases with the ranges of the data from very dry to very wet. Nevertheless, these results are partly supported by our study, which showed that better predictions are obtained when optimization is performed during periods where soil moisture decoupling does not occur. In this respect, given that soil moisture decoupling is accentuated under dry conditions (equation (6)), inverse estimations should be avoided during dry periods. Our investigations also indicated that under dry conditions ET_f is reduced and therefore OF_{et} , driven by the *Feddes et al.* [1978] model, becomes less significant. In section 4.3, it was also shown that for wet periods, during which ET_f remains close to unity (Figure 9c), the sensitivity of OF_{et} is reduced. Thus, the common belief that one requires a period such that θ goes from saturated to residual water content is not supported by this study.

[64] In practical terms, it is recommended that the hydraulic parameters should be preferably optimized after heavy rainfall events, when the soil moisture profile is homogeneous. Nevertheless, the measurements should only start after the plant is starting to experience stress and stopped when the roots are experiencing excessive stress. This finding suggests that the inverse modeling should be

performed during the period where evaporation is not at its maximum, to avoid soil moisture decoupling.

5.2. Comparison of the WOFSA With the Minimum Distance From the Origin

[65] In section 3.1, we mentioned that a well-accepted technique for detecting the optimal value of w , which is a complex trade-off between the information gathered by OF_θ and OF_{et} , is by Minimizing the Euclidean Distance of the Pareto front to the origin (MEDP). Apparently, this requires determining the shape of the Pareto front. In non-linear spaces, this is only achievable by running a suitable multiobjective evolutionary optimization algorithm, which can provide representative nondominated solutions that are uniformly distributed across the objective space [Efstathiadis and Koutsoyiannis, 2010]. For a given shape of the front, the computation of its minimal distance from the origin is trivial. In particular, as illustrated in Figure 1, when OF_θ and OF_{et} are normalized this method results to $w = 0.5$, independently of the values of $\Delta\theta_{rs}$ and ΔET_{rs} , and also independently of the hydroclimatic conditions.

[66] The major drawback of the MEDP approach is the erroneous assumption that the magnitude of $\Delta\theta_{rs}$ is similar to the one of ΔET_{rs} and that the impact of $\Delta\theta_{rs}$ and ΔET_{rs} on the WF is similar. Indeed, our extended investigations within this paper concluded that w is far from constant; on the contrary, it is highly dependent on both the soil texture and climate (Figure 9). Moreover, MEDP fails to take into consideration that when more weight is assigned to OF_θ , then the errors in $\Delta\theta_{rs}$ influences more the computation of the water fluxes and state variables WF, compared to ΔET_{rs} . On the other hand, when more weight is assigned to OF_{et} , the errors in ΔET_r have more influence to the simulated WF, if compared to $\Delta\theta_{rs}$. Hence, the only advantage of MEDP against WOFSA is the simplicity of the computational procedure, but only under the premise that the shape of the Pareto front is well approximated.

5.3. Implementing WOFSA Within a Pareto-Optimization Framework

[67] Forthcoming research needs to address how we can integrate WOFSA within global multiobjective calibration procedures (e.g., MOSCEM, MOPSO, MOHBMO) [Barros et al., 2010], by using real observations. Moreover, it can provide guidance for the selection of the most robust solution, among the mathematically equivalent Pareto optimal alternatives. Indeed, the best-compromise solution of the multiobjective calibration problem is theoretically found in the cross section of the optimally weighted objective function (WOF) and the Pareto-front. Yet, the task of implementing the above idea is nontrivial, since the true water fluxes and state variables (WF_{ref}) are unknown. In the following, we propose preliminary guidelines on how to use WOFSA in a multiobjective calibration setting by assuming that the inverse problem is well posed, thus exhibiting relatively steep trade-offs and that an increase in WOF would produce an increase in WF_{sim} .

5.3.1. Step A: Run Multiobjective Optimization

[68] Perform multiobjective optimization by simultaneous minimizing OF_{et} and OF_θ , for which w does not need to be provided. On the other hand, θ_d which depends on the

climate data can be estimated from Figure 8. During the optimization, all the feasible $HYDRAU_{sim}$ and WF_{sim} which complies with equation (9) are kept in storage which will give the subset of acceptable Pareto-optimal solutions (Figure 1).

5.3.2. Step B: Selection of Temporary Reference Water Fluxes

[69] A first guess of the reference parameters (WF_{ref} , $HYDRAU_{ref}$) is obtained from the cross section of the weighted objective function (WOF) and the subset of Pareto optimal solutions. To obtain a first guess of WOF, w is approximated from Table 8 and θ_d is provided from Figure 8. Next, ΔWF is computed for the subset of acceptable solutions.

5.3.3. Step C: Dividing the Subset of Acceptable Solutions

[70] WOFSA is performed independently on different parts of the subset of acceptable solutions, i.e., the Pareto front (Figure 1). The area is divided on the basis on w . For instance, if the subset of acceptable solutions are divided into four subareas, then the ranges of w are [0; 0.25], [0.25; 0.5], [0.5; 0.75], and [0.75; 1.0]. For each subareas, the WOFSA runs from Step 3, (section 3.3.3), thus obtaining the corresponding \overline{OF}_{lin}^* .

5.3.4. Step D: Refining the Results

[71] The WF_{ref} is updated with the new value of w based on the group which exhibits the lowest \overline{OF}_{lin}^* . Thus, the best-compromise solution is in the cross section of the optimal WOF and the Pareto front (Figure 1). Steps b and c are repeated until convergence occurs between the new optimal w and the previously computed value.

[72] We should remark that although in this study we used two fitting criteria, the WOFSA can be performed with more criteria. In the current version, we suggest using a maximum of four fitting criteria, thus allowing the calibration of up to three weights within the minimization of \overline{OF}_{lin}^* (equation (10b)). The introduction of more criteria would result in a significantly extended Pareto front, tending to cover a large part of the entire objective space. Evidently, this is far from desirable, for both theoretical (i.e., increased uncertainty) and practical reasons (i.e., poor understanding of the generated trade-offs). Nevertheless, very limited are the cases where more than four independent criteria have been applied in real-world applications [Efstathiadis and Koutsoyiannis, 2010]. Forthcoming research will investigate whether is it practical to increase the number of fitting criteria, taking into account that the WOFSA enables to constrain the feasible Pareto front, as depicted in Figure 1, thus significantly facilitating the multiobjective searching procedure.

5.4. The Need for Validation Experiments With Field Data

[73] The proposed WOFSA methodology, which was thoroughly tested on the basis of synthetic data for a wide range of soil texture and climatic conditions, provided consistent and reasonable results. By using synthetic data, we also explicitly ignored uncertainties that are related to field observation errors, thus only focusing to uncertainties due to retrieval of surface soil moisture and evapotranspiration from remote sensing. Evidently, in real-world conditions,

inherent modeling and measurement errors and uncertainties cannot be neglected.

[74] Yet, for a full validation of the methodology, and in order to quantify the gain in accuracy would require the collection of field data. This is by far nontrivial, due to the extent of in situ and remote sensing data requirements as well as potential scaling problems. In fact, performing measurements of effective large-scale water fluxes is considered infeasible because typically θ and ET are retrieved at a scale of several square kilometers. Without considering the scale issues, a way forward can be by using precise weighing lysimeters for which all the water fluxes are continuously monitored (storage, drainage, and evapotranspiration). The surface θ determined (for example) by neutron probe or time-domain reflectometer needs to be monitored. To mimic the uncertainties in retrieving θ and ET from remote sensing, noise can be introduced into the measurements of surface θ and lysimeter ET .

[75] The different lysimeters experiments should contain contrasting textures and climate as described in Figure 2. Preferably, the lysimeters should be filled with representative soils and vegetation. Too dry climates may be avoided since it causes strong surface and root-zone θ decoupling for which these periods can be recognized through the newly introduced threshold θ_d , which is computed from equation (6).

[76] During the validation phase, it is also important to recognize that nondaily information for observed θ and ET is retrieved from thermal-band land surface temperature retrievals, which to date are limited to cloud-free atmospheric conditions [e.g., *Anderson et al.*, 2011]. This implies that the collected data from remote sensing is skewed toward drier conditions.

6. Conclusions

[77] The inversion of the hydraulic parameters of a one-dimensional physically based SVAT model by taking advantage simultaneously of surface soil moisture (θ), and evapotranspiration (ET), requires to take into consideration the uncertainties of retrieving θ and ET from remote sensing and the decoupling of the surface and root-zone θ . To increase the sensitivity of θ , the optimization should not be performed during dry periods, i.e., when decoupling of the surface and root-zone soil moisture occurs. These periods can be recognized through the newly introduced threshold θ_d , which is computed from equation (6).

[78] The proposed multiobjective approach, by means of a weighted objective function (WOF), provides a suitable compromise between fitting criteria against θ and ET , also taking into consideration the contrasting uncertainties in retrieving θ and ET from remote sensing. As shown in the simulations, the uncertainties of θ have different implications in the computation of the water fluxes of interest compared to the uncertainties of ET . WOF comprises of two control variables, namely a weighting coefficient (w) and the decoupling threshold θ_d .

[79] In order to determine the best-compromise values of w and θ_d , we developed a novel inverse modeling framework, called weighted objective function selector algorithm (WOFSA). WOFSA aims to minimize the uncertainties of the computed water fluxes and state variables, following a

systematic and as much as objective procedure, in terms of a theoretical framework for formulating an optimal WOF, on the basis of synthetic data. WOFSA performs forward simulations in order to ensure the greatest linearity between the optimized WOF and the maximum uncertainties of the generated water fluxes ΔWF . The ΔWF are derived by mimicking the typically recommended uncertainties of retrieving θ and ET from remote sensing.

[80] To determine how the optimal w and θ_d of WOF vary under different hydroclimatic conditions, 22 contrasting hydroclimatic scenarios were formulated, by combining five climates, three soil textures, and two different rooting depths. Based on the results provided by WOFSA, we established relationships between the optimized values of w and θ_d . In particular, for all scenarios, we provided empirical relationships to compute θ_d from the average values of θ and ET , and the standard deviation of ET . Moreover, for each texture class, we correlated w with average evaporation fraction and with average surface soil moisture, for which we also provided empirical linear equations. All results are interpreted in terms of hydrological evidence, which is a strong justification of the proposed WOFSA methodology. For instance, we found that θ_d increases for drier hydroclimates and that the rooting depths indirectly influence w through the average evapotranspiration fraction. We remark that typical multiobjective calibration approaches, such as the well-known minimization of the Euclidean Distance of the Pareto set, erroneously assume that the magnitude of $\Delta\theta_{rs}$ is similar to the one of ΔET_{rs} and that the impacts of $\Delta\theta_{rs}$ and ΔET_{rs} on the simulated model responses are not affected by soil and climate conditions.

[81] In practical terms, it is recommended to employ soil moisture measurements preferably after heavy rainfall, when the soil moisture column is homogenized to avoid soil moisture decoupling. Nevertheless, the measurements should be performed only after the plant is starting to experience stress since it was found that the fitting criteria of ET reduces the sensitivity when the Feddes plant water stress response function equals the potential evapotranspiration. The measurements should also not be taken when the plant is experiencing excessive stress, since it reduces the sensitivity of the fitting criteria of ET and causes soil moisture decoupling. It is also advised to perform the study during the season where evaporation is not at its maximum to avoid soil moisture decoupling.

[82] The proposed framework, which was thoroughly tested on the basis of synthetic data for a wide range of soil texture and climatic conditions, provided consistent and reasonable results. Yet, for a full validation of the methodology, and in order to quantify the gain in accuracy without considering the scale issues, a number of calibration experiments with real data are necessary. Evidently, this task is not trivial, mainly because it is very demanding in terms of in situ data measurements, e.g., through high-precision weighing lysimeters.

[83] Our next research step is the implementation of WOFSA within a multiobjective optimization context, taking into account the preliminary ideas of section 5.3. This will enable to reduce the range of the Pareto set in a hydrological perspective, on the basis of real (observed) data across a specific study area. The results of these investigations will be reported in due course.

Appendix A

[84] The appendix describes the sink term and the interception module of SWAP_{inv} which is substantially different than the ones implemented into SWAP.

A1. Potential Evapotranspiration

[85] The potential evapotranspiration ET_p (mm d⁻¹) is estimated by the *Penman and Monteith* equation that was further modified by *Allen et al.* [1998] and is computed by

$$ET_p = \frac{\frac{\Delta v}{\lambda_w}(R_n - G) + \frac{p_1 C_{air} e_{sat} - e_a}{\lambda_w r_{air}}}{\Delta v + \lambda_{air} \left(1 + \frac{r_{crop}}{r_{air}}\right)} \quad (A1)$$

where Δv is the slope of the vapor pressure curve (M L⁻¹ T⁻² θ⁻¹), λ_w is the latent heat of vaporization of water (L² T⁻²), R_n is the net radiation flux density (M T⁻³) above the canopy, G is the soil heat flux density (M T⁻³), p_1 accounts for unit conversion (86,400 s d⁻¹), ρ_{air} is the air density (M T⁻³), C_{air} is the heat capacity of moist air (L T⁻¹ θ⁻¹), e_{sat} is the saturation vapor pressure (M L⁻¹ T⁻²), e_a is the actual vapor pressure (M L⁻¹ T⁻²), r_{air} is the aerodynamic resistance (L⁻¹ T), γ_{air} is the psychrometric constant (M L⁻¹ T⁻² θ⁻¹); and $r_{crop} = 70$ s m⁻¹ is the crop resistance [*Allen, 1986*].

[86] ET_p is partitioned into potential evaporation of the wet canopy E_{PW} (mm d⁻¹), potential soil evaporation E_p (mm d⁻¹) and potential transpiration T_p (mm d⁻¹). The partitioning is performed using the leaf area index LAI (m² m⁻²) and the fraction of the canopy, $1 - F_w$ that is not wet. It is to be noted that F_w is computed differently in SWAP_{inv} (equation (A.15)). SWAP assumes that the net radiation inside the canopy decreases exponentially and that the soil heat is negligible. The partitioning is performed by using a Beer-Lambert law [e.g., *Ritchie, 1972; Goudriaan, 1977; Belmans et al., 1983*]

$$T_p = \max \{ET_p [1 - F_w(E_{pw}, LAI)] - E_p, 0\} \quad (A2)$$

$$E_p = E_{po} F_s \quad (A3)$$

$$F_s = \exp(-K_g LAI) \quad (A4)$$

where F_s (dimensionless) is the interception of solar radiation that will also be used in the interception model, K_g (–) is the extinction coefficient for solar radiation that is set to 0.5 [*Varado et al., 2006; Wang et al., 2009*]. ET_p decreases with increasing K_g and increasing LAI. E_{po} (mm d⁻¹) is the potential evaporation of bare soil, computed for albedo equal to 0.1. For further information on the computation of ET_p , E_{PW} , and E_{po} the readers are referred to the SWAP manual (<http://www.swap.alterra.nl/>).

A2. Sink Term

[87] To take into account tree physiology and the reduction of transpiration by soil water stress, the actual transpiration T is distributed by the sink term $S(h_i)$ over the whole root zone and is calculated for each cell by *Feddes et al.* [1978]. The sink term is computed by

$$S(h_i) = \beta T_p G(h_i) \Delta Rdf_i \quad (A5)$$

where β is the transpiration fraction or crop factor (–), the value of which is provided in Table 5, T_p (mm d⁻¹) (equation (A2)) is the potential transpiration estimated for short grass, ΔRdf_i is the vertical fraction of the root density function per cell i (%) (equation (A6)), and $G(h_i)$ is the reduction of root water uptake at pressure head h per cell i (–) (equation (A8)). All these variables except for T_p are dimensionless.

A2.1. The Root-Density Distribution

[88] In SWAP, the vertical fraction of the root-density function per cell i (ΔRdf_i), which defines the general shape of the roots, is entered manually in tabular form. In SWAP_{inv}, the root distribution is modeled with an empirical function of *Gale and Grigal* [1987] that was modified further by *Pollacco et al.* [2008a]. The model requires the rooting depth and the percentage of root density in the top 30 cm (ΔRdf_{30}). It is to be noted that in this literature the percentage of root density is often stated for the top 30 cm, but the user can specify any other depth. The values of the parameters for the two contrasting scenarios used in this study, composed of shallow and deep rooted plants, are provided in Table 4. For each cell i , the fraction of roots ΔRdf_i between the top depth z_{up} and the bottom depth z_{down} is computed as

$$\Delta Rdf_i = \frac{E_c^{|z_{down}|} - E_c^{|z_{up}|}}{1 - E_c^{|z_{root}|}} \quad \text{with} \quad \sum_1^{i=i_{\max}} \Delta Rdf_i = 1 \quad (A6)$$

where z_{up} and z_{down} are, respectively, the top and bottom depth of each cell which is positive downward (cm). E_c is the “extension coefficient” parameter, z_{root} is the rooting depth (cm), and i_{\max} is the last cell of the root zone. E_c varies between 0.700 and 0.9999, such that when E_c is close to 0.7 all the roots are distributed in the top cell, and when E_c is close to 1, the roots are distributed evenly within the root zone.

[89] The value of E_c is computed from the percentage of roots. For example, in the top 30 cm, ΔRdf_{30} is estimated by solving the following equation:

$$\Delta Rdf_{30} = \frac{E_c^0 - E_c^{30}}{1 - E_c^{|z_{root}|}} = \frac{1 - E_c^{30}}{1 - E_c^{|z_{root}|}} \quad (A7)$$

where E_c is the “extension coefficient” parameter and z_{root} is the rooting depth (cm).

A2.2. Root Water Uptake

[90] When the capillary pressure head h_i per node i is reduced, the vegetation closes their stoma and decreases transpiration, by using the *Feddes et al.* [1978] stress function computed as follows:

$$\begin{aligned} G(h_i) &= 0, \quad \text{if } |h| > |h_4| \text{ or } |h| < |h_1| \\ G(h_i) &= 1, \quad \text{if } |h| > |h_2| \text{ and } |h| < |h_3| \end{aligned} \quad (A8)$$

[91] Water uptake below $|h_1|$ (oxygen deficiency) and above $|h_4|$ (wilting point) is set to zero. Between $|h_2|$ and $|h_3|$, $g(h_i) = T_p$ maximal. The value of h_3 varies with T_p . For different values of T_p , h_3 is linearly interpolated between h_{3low} and h_{3high} . The values of h_1 , h_2 , h_{3high} , h_{3low} , and h_4 are provided in Table 5.

A3. Evaporation From Bare Soil

[92] The evaporation module of SWAP was simplified. Under wet soil conditions, the actual soil evaporation E [mm d^{-1}] equals the potential soil evaporation E_p . During interstorm period SWAP computes E by using the empirical evaporation method of *Black et al.* [1969] that requires two fitting parameters. Nevertheless *Eagleson* [1978], *Milly* [1986], *Simmons and Meyer* [2000], and *Romano and Giudici* [2007, 2009] showed that good results can be achieved by relating evaporation with θ . We therefore used the *Romano and Giudici* [2007, 2009] evaporation model that does not require any extra parameters

$$E = \frac{\text{MAX} \theta \left| \begin{array}{l} 0 \\ 15 \end{array} - \theta_r \right.}{\theta_s - \theta_r} E_p \quad (\text{A9})$$

where the maximum θ is taken from the highest soil moisture between the surface and the depth to 15 cm; θ_r and θ_s are the residual and saturated water contents ($\text{L}^3 \text{L}^{-3}$), respectively, defined earlier by equation (3).

A4. Rainfall Interception Model

[93] SWAP computes rainfall interception following *Braden* [1985] and *Von Hoyningen-Huene* [1981]. These interception models require extra parameters and do not use potential evaporation of a wet canopy E_{pw} (mm d^{-1}). We introduced in SWAP_{inv} a physically based interception model, following the work of *Noilhan and Lacarrere* [1995] and *Varado et al.* [2006] described in *Pollacco and Mohanty* [2012]. In this model, E_{pw} is used as a predictor, while the leaf area index LAI (–) and the extinction coefficient of solar radiation K_g (–) are assumed as parameters. The values of the LAI and K_g are provided in Table 5. The gross precipitation P_g (mm d^{-1}) defined as the amount of water which reaches the canopy is computed following *Rutter et al.* [1971]

$$P_g = P_{int} + P_{free} \quad (\text{A10})$$

where P_{free} (mm d^{-1}) is the free throughfall that is the fraction of precipitation that reaches the ground surface through gaps in the canopy and P_{int} (mm d^{-1}) is the intercepted precipitation.

[94] The foliage of the canopy is considered as a water reservoir filled up to a depth of W_r (mm), with a maximum storage capacity W_{max} (mm). When the canopy is fully saturated ($W_r = W_{max}$), then any excess of P_{int} overflows P_{over} (mm) to the ground such that according to *Valante et al.* [1997]

$$P_{over} = \max \{P_{int} + W_r - W_{max}, 0\} \quad (\text{A11})$$

[95] The amount of water that reaches the ground is the net precipitation P_{net} (mm d^{-1})

$$P_{net} = P_{over} + P_{free} \quad (\text{A12})$$

[96] A fraction of the water from the reservoir W_r will be evaporated at the rate of the actual evaporation of a wetted canopy EA_w (mm d^{-1}) during and after a rainfall event. W_r is calculated following *Deardorff* [1978]

$$\partial W_r / \partial t = P_{int} - P_{over} - EA_w \quad (\text{A13})$$

[97] The maximum quantity of water that can be evaporated during a time step is computed as

$$EA_w = \min \{E_{pw} F_w, W_r / dt\} \quad (\text{A14})$$

where E_{pw} is the potential transpiration of a wet canopy.

[98] According to *Rutter et al.* [1971], evaporation from wet canopies is assumed to be proportional to the fraction of the canopy that is wet F_w (0–1) that is computed following *Deardorff* [1978]

$$F_w = (W_r / W_{max})^{2/3} \quad (\text{A15})$$

[99] W_{max} is related to LAI based on the empirical relationship of *Varado et al.* [2006] and *Von Hoyningen-Huene* [1981]. *Varado et al.* [2006] assumes that the interception of water of a canopy is similar to the interception of solar radiation F_s (0–1) (equation (A.4)). Combining *Varado et al.* [2006] and *Von Hoyningen-Huene* [1981], W_{max} is computed as

$$W_{max} = (0.935 + 0.498 \text{ LAI} - 0.00575 \text{ LAI}^2) (1 - F_s) \quad (\text{A16})$$

[100] W_{max} increases with increasing LAI and K_g . The partitioning of P_g and P_{free} is computed as

$$P_{free} = F_s P_g \quad (\text{A17})$$

$$P_{int} = (1 - F_s) P_g \quad (\text{A18})$$

$$F_s = e^{-K_g \text{ LAI}} \quad (\text{A19})$$

[101] **Acknowledgments.** We acknowledge the partial support of National Science Foundation (CMG/DMS grant 062113 and 0934837) and NASA THPs (NNX08AF55G and NNX09AK73G) grants. We are thankful for Kroes Joop (ALTERRA, Netherlands), Jos van Dam (ALTERRA, Netherlands), Isabelle Braud (CEMAGREF, France), Rafael Angulo (ENTPE, France), and Edwin Norbeck (Dept. of Physics and Astronomy, University of Iowa) for their suggestions during the course of this study, as well as Martha Anderson (USDA-ARS Hydrology and Remote Sensing Lab, Beltsville, MD, USA), for her assistance with questions on the uncertainties in retrieving soil moisture from remote sensing. We would also like to thank the three reviewers as well as the Associate Editor, Alberto Montanari, for their constructive comments and critique, which helped us providing a much improved paper.

References

- Allen, R. G. (1986), A Penman for all seasons, *J. Irrig. Drain. Eng.*, 112(4), 348–368.
- Allen, R. G., L. S. Pereira, D. Raes, and M. Smith (1998), *Crop Evapotranspiration, Guidelines for Computing Crop Water Requirements*, FAO, Rome.
- Anderson, M. C., C. Hain, B. Wardlow, A. Pimstein, J. R. Mecikalski, and W. P. Kustas (2011), Evaluation of drought indices based on thermal remote sensing of evapotranspiration over the continental United States, *J. Clim.*, 24, 2025–2044.
- Barros, F. V. F., E. S. P. R. Martins, L. S. V. Nascimento, and D. S. Reis Jr (2010), Use of multiobjective evolutionary algorithms in water resources engineering, in *Multi-Objective Swarm Intelligent Systems, Theory & Experiences, Studies in Computational Intelligence*, vol. 261, edited by

- N. Nedjah, L. dos Santos Coelho, and L. de Macedo de Mourelle, chap. 3, pp. 45–82, Springer, Berlin.
- Bashir, M. A., H. Tanakamaru, and A. Tada (2009), Spatial and temporal analysis of evapotranspiration using satellite remote sensing data: A case study in the Gezira Scheme, *Sudan, J. Environ. Inf.*, 13(2), 86–92.
- Bastidas, L. A., H. V. Gupta, S. Sorooshian, W. J. Shuttleworth, and Z. L. Yang (1999), Sensitivity analysis of a land surface scheme using multi-criteria methods, *J. Geophys. Res.*, 104(D16), 19,481–19,490.
- Belmans, C., J. G. Wesseling, and R. A. Feddes (1983), Simulation model of the water balance of a cropped soil: SWATRE, *J. Hydrol.*, 63(3–4), 271–286.
- Bindlish, R., T. J. Jackson, A. J. Gasiewski, M. Klein, and E. G. Njoku (2006), Soil moisture mapping and AMSR-E validation using the PSR in SMEX02, *Remote Sens. Environ.*, 103(2), 127–139.
- Black, T. A., W. R. Gardner, and G. W. Thurtell (1969), The prediction of evaporation, drainage, and soil water storage for a bare soil, *Soil Sci. Soc. Am. Proc.*, 33, 655–660.
- Boufadel, M. C., M. T. Suidan, A. D. Venosa, C. H. Rauch, and P. Biswas (1998), 2d variably saturated flows: Physical scaling and Bayesian estimation, *J. Hydrol. Eng.*, 3(4), 223–231.
- Braden, H. (1985), Ein Energiehaushalts- und Verdunstungsmodell für Wasser- und Stoffhaushaltsuntersuchungen landwirtschaftlich genutzter Einzugsgebiete, *Mitt. Dtsch. Bodenkdl. Ges.*, 42, 294–299.
- Brutsaert, W. (2005), *Hydrology: An Introduction*, 605 pp., Cambridge Univ. Press, Cambridge, U. K.
- Capehart, W. J., and T. N. Carlson (1997), Decoupling of surface and near-surface soil water content: A remote sensing perspective, *Water Resour. Res.*, 33(6), 1383–1395.
- Carsel, R. F., and R. S. Parrish (1988), Developing joint probability distributions of soil-water retention characteristics, *Water Resour. Res.*, 24(5), 755–769.
- Choi, M., J. M. Jacobs, and D. D. Bosch (2008), Remote sensing observatory validation of surface soil moisture using Advanced Microwave Scanning Radiometer E, Common Land Model, and ground based data: Case study in SMEX03 Little River Region, Georgia, U.S., *Water Resour. Res.*, 44, W08421, doi:10.1029/2006WR005578.
- Coudert, B., C. Otle, B. Boudevillain, J. Demarty, and P. Guillevic (2006), Contribution of thermal infrared remote sensing data in multiobjective calibration of a dual-source SVAT model, *J. Hydrometeorol.*, 7(3), 404–420.
- Crispim, J. A., and J. P. de Sousa (2009), Partner selection in virtual enterprises: A multi-criteria decision support approach, *Int. J. Prod. Res.*, 47(17), 4791–4812.
- Das, N. N., B. P. Mohanty, M. H. Cosh, and T. J. Jackson (2008), Modeling and assimilation of root zone soil moisture using remote sensing observations in Walnut Gulch Watershed during SMEX04, *Remote Sens. Environ.*, 112(2), 415–429.
- Davenport, I. J., J. Fernandez-Galvez, and R. J. Gurney (2005), A sensitivity analysis of soil moisture retrieval from the Tau-Omega microwave emission model, *IEEE Trans. Geosci. Remote Sens.* 43(6), 1304–1316.
- De Lannoy, G. J. M., P. R. Houser, V. R. N. Pauwels, and N. E. C. Verhoest (2007), State and bias estimation for soil moisture profiles by an ensemble Kalman filter: Effect of assimilation depth and frequency, *Water Resour. Res.*, 43, W06401, doi:10.1029/2006WR005100.
- Deardorff, J. W. (1978), Efficient prediction of ground surface-temperature and moisture, with inclusion of a layer of vegetation, *J. Geophys. Res.*, 83(C4), 1889–1903.
- Deb, K., and H. Gupta (2005), Searching for robust Pareto-optimal solutions in multi-objective optimization, in *Evolutionary Multi-Criterion Optimization, Lecture Notes in Computer Science*, vol. 3410, pp. 150–164, Springer, Berlin.
- Demarty, J., C. Otle, I. Braud, A. Olioso, J. P. Frangi, L. A. Bastidas, and H. V. Gupta (2004), Using a multiobjective approach to retrieve information on surface properties used in a SVAT model, *J. Hydrol.*, 287(1–4), 214–236.
- Demarty, J., C. Otle, I. Braud, A. Olioso, J. P. Frangi, H. V. Gupta, and L. A. Bastidas (2005), Constraining a physically based Soil-Vegetation-Atmosphere Transfer model with surface water content and thermal infrared brightness temperature measurements using a multiobjective approach, *Water Resour. Res.*, 41, W01011, doi:10.1029/2004WR003695.
- Duan, Q. Y., S. Sorooshian, and V. Gupta (1992), Effective and efficient global optimization for conceptual rainfall-runoff models, *Water Resour. Res.*, 28(4), 1015–1031.
- Duan, Q. Y., S. Sorooshian, and V. K. Gupta (1994), Optimal use of the SCE-UA global optimization method for calibrating watershed models, *J. Hydrol.*, 158(3–4), 265–284.
- Dumedah, G., A. A. Berg, M. Wineberg, and R. Collier (2010), Selecting model parameter sets from a trade-off surface generated from the non-dominated sorting genetic algorithm-II, *Water Resour. Manage.*, 24(15), 4469–4489.
- Dumedah, G., A. A. Berg, and M. Wineberg (2012a), Pareto-optimality and a search for robustness: Choosing solutions with desired properties in objective space and parameter space, *J. Hydroinf.*, 14(2), 270–285.
- Dumedah, G., A. Berg, and M. Wineberg (2012b), Evaluating auto-selection methods used for choosing solutions from Pareto-optimal set: Does non-dominance persist from calibration to validation phase?, *J. Hydrol. Eng.*, 17(1), 150–159.
- Eagleson, P. S. (1978), Climate, soil and vegetation: 1. Introduction to water balance dynamics, *Water Resour. Res.*, 14(5), 705–712.
- Efstratiadis, A., and D. Koutsoyiannis (2010), One decade of multiobjective calibration approaches in hydrological modelling: A review, *Hydrol. Sci. J.*, 55(1), 58–78.
- Entekhabi, D., et al. (2010), The soil moisture active passive (SMAP) mission, *Proc. IEEE*, 98(5), 704–716.
- Feddes, R. A., P. J. Kowalik, and H. Zaradny (1978), *Simulation of Field Water Use and Crop Yield*, Simulation Monographs, 188 pp., John Wiley, Australia.
- Feddes, R. A., M. Menti, P. Kabat, and W. G. M. Bastiaanssen (1993), Is large-scale inverse modelling of unsaturated flow with areal average evaporation and surface soil moisture as estimated from remote sensing feasible?, *J. Hydrol.*, 143(1–2), 125–152.
- Fernández-Gálvez, J. (2008), Errors in soil moisture content estimates induced by uncertainties in the effective soil dielectric constant, *Int. J. Remote Sens.*, 29(11), 3317–3323.
- Franks, S. W., K. J. Beven, and J. H. C. Gash (1999), Multi-objective conditioning of a simple SVAT model, *Hydrol. Earth Syst. Sci.*, 3(4), 477–489.
- Gale, M. R., and D. F. Grigal (1987), Vertical root distributions of northern tree species in relation to successional status, *Can. J. Forest Res.*, 17(8), 829–834.
- Gao, Y. C., and D. Long (2008), Intercomparison of remote sensing-based models for estimation of evapotranspiration and accuracy assessment based on SWAT, *Hydrol. Processes*, 22(25), 4850–4869.
- Goudriaan, J. (1977), *Crop Micrometeorology: A Simulation Study*, Simulation monographs, Pudoc, Wageningen.
- Gupta, H. V., S. Sorooshian, and P. O. Yapo (1998), Toward improved calibration of hydrologic models: Multiple and noncommensurable measures of information, *Water Resour. Res.*, 34(4), 751–763.
- Gupta, H. V., L. A. Bastidas, S. Sorooshian, W. J. Shuttleworth, and Z. L. Yang (1999), Parameter estimation of a land surface scheme using multi-criteria methods, *J. Geophys. Res.*, 104(D16), 19,491–19,503.
- Gutmann, E. D., and E. E. Small (2010), A method for the determination of the hydraulic properties of soil from MODIS surface temperature for use in land-surface models, *Water Resour. Res.*, 46, W06520, doi:10.1029/2009WR008203.
- Haverkamp, R., F. J. Leij, C. Fuentes, A. Sciortino, and P. J. Ross (2005), Soil water retention: I. Introduction of a shape index, *Soil Sci. Soc. Am. J.*, 69(6), 1881–1890.
- Hong, S. H., J. M. H. Hendrickx, and B. Borchers (2009), Up-scaling of SEBAL derived evapotranspiration maps from Landsat (30 m) to MODIS (250 m) scale, *J. Hydrol.*, 370(1–4), 122–138.
- Huete, A., K. Didan, T. Miura, E. P. Rodriguez, X. Gao, and L. G. Ferreira (2002), Overview of the radiometric and biophysical performance of the MODIS vegetation indices, *Remote Sens. Environ.*, 83(1–2), 195–213.
- Ines, A. V. M., and P. Droogers (2002), Inverse modelling in estimating soil hydraulic functions: A Genetic Algorithm approach, *Hydrol. Earth Syst. Sci.*, 6(1), 49–65.
- Ines, A. V. M., and B. P. Mohanty (2008a), Near-surface soil moisture assimilation for quantifying effective soil hydraulic properties under different hydroclimatic conditions, *Vadose Zone J.*, 7(1), 39–52.
- Ines, A. V. M., and B. P. Mohanty (2008b), Near-surface soil moisture assimilation for quantifying effective soil hydraulic properties using genetic algorithm: 1. Conceptual modeling, *Water Resour. Res.*, 44, W06422, doi:10.1029/2007WR005990.
- Ines, A. V. M., and B. P. Mohanty (2008c), Parameter conditioning with a noisy Monte Carlo genetic algorithm for estimating effective soil hydraulic properties from space, *Water Resour. Res.*, 44, W08441, doi:10.1029/2007WR006125.

- Ines, A. V. M., and B. P. Mohanty (2009), Near-surface soil moisture assimilation for quantifying effective soil hydraulic properties using genetic algorithms: 2. Using airborne remote sensing during SGP97 and SMEX02, *Water Resour. Res.*, 45, W01408, doi:10.1029/2008WR007022.
- Jackson, T. J., and T. J. Schugge (1991), Vegetation effects on the micro-wave emission of soils, *Remote Sens. Environ.*, 36(3), 203–212.
- Jackson, R. B., J. Canadell, J. R. Ehleringer, H. A. Mooney, O. E. Sala, and E. D. Schulze (1996), A global analysis of root distributions for terrestrial biomes, *Oecologia*, 108(3), 389–411.
- Jhorar, R. K., W. G. M. Bastiaanssen, R. A. Feddes, and J. C. Van Dam (2002), Inversely estimating soil hydraulic functions using evapotranspiration fluxes, *J. Hydrol.*, 258(1–4), 198–213.
- Jhorar, R. K., J. C. van Dam, W. G. M. Bastiaanssen, and R. A. Feddes (2004), Calibration of effective soil hydraulic parameters of heterogeneous soil profiles, *J. Hydrol.*, 285(1–4), 233–247.
- Kalma, J. D., T. R. McVicar, and M. F. McCabe (2008), Estimating land surface evaporation: A review of methods using remotely sensed surface temperature data, *Surv. Geophys.*, 29(4–5), 421–469.
- Kerr, Y. H., P. Waldteufel, J. P. Wigneron, J. M. Martinuzzi, J. Font, and M. Berger (2001), Soil moisture retrieval from space: The Soil Moisture and Ocean Salinity (SMOS) mission, *IEEE Trans. Geosci. Remote Sens.*, 39(8), 1729–1735.
- Khu, S. T., and H. Madsen (2005), Multiobjective calibration with Pareto preference ordering: An application to rainfall-runoff model calibration, *Water Resour. Res.*, 41, W03004, doi:10.1029/2004WR003041.
- Kroes, J. G., J. G. Wesseling, and J. C. Van Dam (2000), Integrated modeling of the soil-water-atmosphere-plant system using the model SWAP 2.0 an overview of theory and an application, *Hydrol. Processes*, 14(11–12), 1993–2002.
- Laumanns, M., L. Thiele, K. Deb, and E. Zitzler (2002), Combining convergence and diversity in evolutionary multiobjective optimization, *Evol. Comput.*, 10(3), 263–282.
- Leij, F. J., W. J. Alves, M. T. Van Genuchten, and J. R. Williams (1996), The UNSODA Unsaturated Soil Hydraulic Database, User's Manual, Version 1.0, EPA/600/R-96/095, 103 pp., Natl. Risk Manage. Lab., Off. of Res. and Dev., U.S. Environ. Prot. Agency (EPA), Cincinnati, OH.
- Li, F., W. P. Kustas, M. C. Anderson, T. J. Jackson, R. Bindlish, and J. H. Prueger (2006), Comparing the utility of microwave and thermal remote-sensing constraints in two-source energy balance modeling over an agricultural landscape, *Remote Sens. Environ.*, 101(3), 315–328.
- Luckner, L., M. T. Van Genuchten, and D. R. Nielsen (1989), A consistent set of parametric models for the two-phase flow of immiscible fluids in the subsurface, *Water Resour. Res.*, 25(10), 2187–2193.
- Madsen, H. (2003), Parameter estimation in distributed hydrological catchment modelling using automatic calibration with multiple objectives, *Adv. Water Resour.*, 26(2), 205–216.
- Milly, P. C. D. (1986), An event-based simulation model of moisture and energy fluxes at a bare soil surface, *Water Resour. Res.*, 22(12), 1680–1692.
- Mo, X. G., S. X. Liu, Z. Lin, X. Sun, and Z. Zhu (2006), Multi-objective conditioning of a SVAT model for heat and CO₂ fluxes prediction, in *Prediction in Ungauged Basins: Promises and Progress (Proceedings of symposium S7 held during the Seventh IAHS Scientific)*, edited by M. Sivapalan, et al., pp. 164–176, IAHS Publ., Assembly at Foz do Iguaçu, Brazil.
- Mohanty, B. P., and J. Zhu (2007), Effective hydraulic parameters in horizontally and vertically heterogeneous soils for steady-state land-atmosphere interaction, *J. Hydrometeorol.*, 8(4), 715–729.
- Mroczkowski, M., G. P. Raper, and G. Kuczera (1997), The quest for more powerful validation of conceptual catchment models, *Water Resour. Res.*, 33(10), 2325–2335.
- Mualem, Y. (1976), A new model for predicting the hydraulic conductivity of unsaturated porous media, *Water Resour. Res.*, 12(3), 513–522.
- Naeimi, V., K. Scipal, Z. Bartalis, S. Hasenauer, and W. Wagner (2009), An improved soil moisture retrieval algorithm for ERS and METOP scatterometer observations, *IEEE Trans. Geosci. Remote Sens.*, 47(7), 1999–2013.
- Nagler, P. L., J. Cleverly, E. Glenn, D. Lampkin, A. Huete, and Z. M. Wan (2005), Predicting riparian evapotranspiration from MODIS vegetation indices and meteorological data, *Remote Sens. Environ.*, 94(1), 17–30.
- Njoku, E. G., and S. K. Chan (2006), Vegetation and surface roughness effects on AMSR-E land observations, *Remote Sens. Environ.*, 100(2), 190–199.
- Noilhan, J., and P. Lacarrere (1995), GCM grid-scale evaporation from mesoscale modeling, *J. Clim.*, 8(2), 206–223.
- Opoku-Duah, S., D. N. M. Donoghue, and T. P. Burt (2008), Intercomparison of evapotranspiration over the Savannah Volta Basin in West Africa using remote sensing data, *Sensors*, 8(4), 2736–2761.
- Pollacco, J. A. P. (2005), Inverse methods to determine parameters in a physically-based model of soil water balance, 190 pp., Univ. of Newcastle upon Tyne, Newcastle upon Tyne, U. K.
- Pollacco, J. A. P., and B. P. Mohanty (2012), Uncertainties of water fluxes in soil-vegetation-atmosphere transfer models: Inverting surface soil moisture and evapotranspiration retrieved from remote sensing, *Vadose Zone J.*, 11(3), doi:10.2136/vzj2011.0167.
- Pollacco, J. A. P., I. Braud, R. Angulo-Jaramillo, and B. Saugier (2008a), A Linking Test that establishes if groundwater recharge can be determined by optimising vegetation parameters against soil moisture, *Ann. Forest Sci.*, 65(7), 702, doi:10.1051/forest:2008046.
- Pollacco, J. A. P., J. M. S. Ugalde, R. Angulo-Jaramillo, I. Braud, and B. Saugier (2008b), A linking test to reduce the number of hydraulic parameters necessary to simulate groundwater recharge in unsaturated soils, *Adv. Water Resour.*, 31(2), 355–369.
- Ramos, J. G., C. R. Cratchley, J. A. Kay, M. A. Casterad, A. Martinez-Cob, and R. Dominguez (2009), Evaluation of satellite evapotranspiration estimates using ground-meteorological data available for the Flumen District into the Ebro Valley of N.E. Spain, *Agric. Water Manage.*, 96(4), 638–652.
- Reed, P., B. S. Minsker, and D. E. Goldberg (2003), Simplifying multiobjective optimization: An automated design methodology for the Nondominated Sorted Genetic Algorithm-II, *Water Resour. Res.*, 39(7), 1196, doi:10.1029/2002WR001483.
- Refsgaard, J. C., and B. Storm (1996), Construction, calibration and validation of hydrological models, in *Distributed Hydrological Modelling*, edited by M. B. Abbott and J. C. Refsgaard, pp. 41–54, Kluwer Academic Press: The Netherlands.
- Ritchie, J. T. (1972), Model for predicting evaporation from a row crop with incomplete cover, *Water Resour. Res.*, 8(5), 1204–1213.
- Romano, E., and M. Giudici (2007), Experimental and modeling study of the soil-atmosphere interaction and unsaturated water flow to estimate the recharge of a phreatic aquifer, *J. Hydrol. Eng.*, 12(6), 573–584.
- Romano, E., and M. Giudici (2009), On the use of meteorological data to assess the evaporation from a bare soil, *J. Hydrol.*, 372(1–4), 30–40.
- Russo, D. (1988), Determining soil hydraulic properties by parameter estimation: On the selection of a model for the hydraulic properties, *Water Resour. Res.*, 24(3), 453–459.
- Rutter, A. J., K. A. Kershaw, P. C. Robins, and A. J. Morton (1971), A predictive model of rainfall interception in forests, 1. Derivation of the model from observations in a plantation of Corsican pine, *Agric. Meteorol.*, 9(C), 367–384.
- Sahoo, A. K., P. R. Houser, C. Ferguson, E. F. Wood, P. A. Dirmeyer, and M. Kafatos (2008), Evaluation of AMSR-E soil moisture results using the in-situ data over the Little River Experimental Watershed, Georgia, *Remote Sens. Environ.*, 112(6), 3142–3152.
- Schaap, M. G., and F. J. Leij (1998), Using neural networks to predict soil water retention and soil hydraulic conductivity, *Soil Tillage Res.*, 47(1–2), 37–42.
- Schenk, H. J., and R. B. Jackson (2002), The global biogeography of roots, *Ecol. Monogr.*, 72(3), 311–328.
- Shin, Y., B. P. Mohanty, and A. V. M. Ines (2012), Soil hydraulic properties in one-dimensional layered soil profile using layer-specific soil moisture assimilation scheme, *Water Resour. Res.*, 48, W06529, doi:10.1029/2010WR009581.
- Simic, A., R. Fernandes, R. Brown, P. Romanov, and W. Park (2004), Validation of VEGETATION, MODIS, and GOES + SSM/I snow-cover products over Canada based on surface snow depth observations, *Hydrol. Processes*, 18(6), 1089–1104.
- Simmons, C. S., and P. D. Meyer (2000), A simplified model for the transient water budget of a shallow unsaturated zone, *Water Resour. Res.*, 36(10), 2835–2844.
- Simmonds, L. P., et al. (2004), Soil moisture retrieval by a future spaceborne Earth observation mission, *Eur. Space Agency Contract Rep.*, Univ. of Reading, Reading, U. K.
- Singh, R., J. G. Kroes, J. C. van Dam, and R. A. Feddes (2006), Distributed ecohydrological modelling to evaluate the performance of irrigation system in Sirsa district, India: I. Current water management and its productivity, *J. Hydrol.*, 329(3–4), 692–713.
- Sun, R., J. Shi, and L. Jiang (2007), A method to retrieve soil moisture using ERS Scatterometer data, Geoscience and Remote Sensing Symposium (IGARSS 2007), *IEEE Int.*, 1857–1860.

- Taboada, H., and D. Coit (2006), Data mining techniques to facilitate the analysis of the Pareto-optimal set for multiple objective problems, paper presented at Industrial Engineering Research Conference (IERC), Orlando, Fla.
- Teixeira, A. H. d. C., W. G. M. Bastiaanssen, M. D. Ahmad, and M. G. Bos (2009a), Reviewing SEBAL input parameters for assessing evapotranspiration and water productivity for the Low-Middle Sao Francisco River basin, Brazil. Part B: Application to the regional scale, *Agric. Forest Meteorol.*, 149(3–4), 477–490.
- Teixeira, A. H. d. C., W. G. M. Bastiaanssen, M. D. Ahmad, and M. G. Bos (2009b), Reviewing SEBAL input parameters for assessing evapotranspiration and water productivity for the Low-Middle São Francisco River basin, Brazil. Part A: Calibration and validation, *Agric. Forest Meteorol.*, 149(3–4), 462–476.
- Tietje, O., and M. Tapkenhriehs (1993), Evaluation of pedo-transfer functions, *Soil Sci. Soc. Am. J.*, 57(4), 1088–1095.
- Twarakavi, N. K. C., H. Saito, J. Simunek, and M. T. van Genuchten (2008), A new approach to estimate soil hydraulic parameters using only soil water retention data, *Soil Sci. Soc. Am. J.*, 72(2), 471–479.
- Valante, F., J. S. David, and J. H. C. Gash (1997), Modelling interception loss for two sparse eucalypt and pine forests in central Portugal using reformulated Rutter and Gash analytical models, *J. Hydrol.*, 190(1–2), 141–162.
- Van Dam, J. C. (2000), Field-scale water flow and solute transport, SWAP model concepts, parameter estimation, and case studies. PhD thesis, 167 pp., Wageningen University, Wageningen, The Netherlands.
- Van Dam, J. C., J. Huygen, J. G. Wesseling, R. A. Feddes, P. Kabat, P. E. V. Van Walsum, P. Groenendijk, and C. A. Van Diepen (1997), Theory of SWAP Version 2.0. Simulation of Water Flow, Solute Transport and Plant Growth in the Soil-Water-Atmosphere-Plant Environment, Tech. Doc. 45, DLO Winand Staring Cent., Wageningen, Netherlands.
- Van Dam, J. C., P. Groenendijk, R. F. A. Hendriks, and J. G. Kroes (2008), Advances of modeling water flow in variably saturated soils with SWAP, *Vadose Zone J.*, 7(2), 640–653.
- van Genuchten, M. T. (1980), Closed-form equation for predicting the hydraulic conductivity of unsaturated soils, *Soil Sci. Soc. Am. J.*, 44(5), 892–898.
- van Griensven, A., and T. Meixner (2006), Methods to quantify and identify the sources of uncertainty for river basin water quality models, *Water Sci. Technol.*, 53(1), 51–59.
- Varado, N., I. Braud, and P. J. Ross (2006), Development and assessment of an efficient vadose zone module solving the 1D Richards' equation and including root extraction by plants, *J. Hydrol.*, 323(1–4), 258–275.
- Vegas Galdos, F., C. Álvarez, A. García, and J. A. Revilla (2012), Estimated distributed rainfall interception using a simple conceptual model and Moderate Resolution Imaging Spectroradiometer (MODIS), *J. Hydrol.*, 468–469, 213–228.
- Verstraeten, W. W., F. Veroustraete, and J. Feyen (2008), Assessment of evapotranspiration and soil moisture content across different scales of observation, *Sensors*, 8(1), 70–117.
- Vischel, T., G. G. S. Pegram, S. Sinclair, W. Wagner, and A. Bartsch (2008), Comparison of soil moisture fields estimated by catchment modelling and remote sensing: A case study in South Africa, *Hydrol. Earth Syst. Sci.*, 12(3), 751–767.
- Von Hoyningen-Huene, J. (1981), *Die Interzeption des Niederschlags in Landwirtschaftlichen Pflanzenbeständen*, Arbeitsbericht Deutscher verband fur Wasserwirtschaft und Kulturbau, Braunschwig, Germany.
- Vrugt, J. A., W. Bouten, H. V. Gupta, and S. Sorooshian (2002), Toward improved identifiability of hydrologic model parameters: The information content of experimental data, *Water Resour. Res.*, 38(12), 48-1-48-13.
- Walker, J. P., G. R. Willgoose, and J. D. Kalma (2002), Three-dimensional soil moisture profile retrieval by assimilation of near-surface measurements: Simplified Kalman filter covariance forecasting and field application, *Water Resour. Res.*, 38(12), 1–18.
- Wang, C., P. Wang, X. Zhu, W. Zheng, and H. Yang (2008), Estimations of evapotranspiration and surface soil moisture based on remote sensing data and influence factors, *Nongye Gongcheng Xuebao/Trans. Chin. Soc. Agric. Eng.*, 24(10), 127–133.
- Wang, T., V. A. Zlotnik, J. Simunek, and M. G. Schaap (2009), Using pedo-transfer functions in vadose zone models for estimating groundwater recharge in semiarid regions, *Water Resour. Res.*, 45(4), W04412, doi:10.1029/2008WR006903.
- Wilson, D. J., A. W. Western, R. B. Grayson, A. A. Berg, M. S. Lear, M. Rodell, J. S. Famiglietti, R. A. Woods, and T. A. McMahon (2003), Spatial distribution of soil moisture over 6 and 30 cm depth, Mahurangi river catchment, New Zealand, *J. Hydrol.*, 276(1–4), 254–274.
- Wu, B. F., J. Xiong, N. N. Yan, L. D. Yang, and X. Du (2008), ETWatch for monitoring regional evapotranspiration with remote sensing, *Shuikexue Jinzhan/Adv. Water Sci.*, 19(5), 671–678.
- Yapo, P. O., H. V. Gupta, and S. Sorooshian (1998), Multi-objective global optimization for hydrologic models, *J. Hydrol.*, 204(1–4), 83–97.
- Zhan, X. W., W. T. Crow, T. J. Jackson, and P. E. O'Neill (2008), Improving spaceborne radiometer soil moisture retrievals with alternative aggregation rules for ancillary parameters in highly heterogeneous vegetated areas, *IEEE Geosci. Remote Sens. Lett.*, 5(2), 261–265.
- Zhang, X., S. Kang, P. Wang, and L. Tong (2006), Comparative analysis of regional evapotranspiration estimation models using remotely sensed data, *Nongye Gongcheng Xuebao/Trans. Chin. Soc. Agric. Eng.*, 22(7), 6–13.